Carbon Sequestration and Enhanced Hydrocarbon Recovery: Ultrasonics Vp and Vs and Laboratory Fluid Replacement for the Mississippian Carbonates, Wellington Field, Kansas

by

Matilda Awo King

B.S., University of Ghana, 2019

A THESIS

submitted in partial fulfillment of the requirements for the degree

MASTER OF SCIENCE

Department of Geology
College of Arts and Sciences

KANSAS STATE UNIVERSITY
Manhattan, Kansas

2025

Approved by:

Major Professor
Dr Abdelmoneam Raef

Copyright

Abstract

The feasibility of enhanced oil recovery (EOR) and carbon geosequestration for the Mississippian carbonates of south-central Kansas remains an important endeavor. This depleting reservoir formation has heterogeneous lithofacies, variable pore structures, and potentially pore-fluid composition of variable seismic signatures. Understanding the elastic properties of these carbonates is crucial for assessing their reservoir qualities through optimizing fluid injection strategies and conducting insightful seismic modeling. This study employs ultrasonic velocity measurements to investigate the elastic moduli of Mississippian carbonates, understand the response of P- and S-waves to pore fluid changes, and contribute assessing the suitability of these formations for long-term CO_2 storage and EOR programs. An ultrasonic laboratory system was used to measure compressional (P-wave) and shear (S-wave) velocities under both dry and fluid-saturated conditions, while porosity was determined using a porosimeter. Additionally, fluid substitution modeling was performed to analyze how different pore fluids influence wave propagation. The results indicate that traditional velocity analysis alone may not be sufficient for fluid discrimination in reservoirs. Instead, attenuation measurements proved to be a more reliable attribute for distinguishing between pore fluids, highlighting its potential application in monitoring reservoir conditions during EOR operations. These findings suggest that attenuation-based analyses could improve the identification of dry reservoirs and enhance the detection of fluid migration during injection processes. Furthermore, the favorable elastic properties of the Mississippian carbonates, including their ability to retain mechanical integrity under varying saturation conditions, support their viability as candidates for both hydrocarbon recovery and CO_2 sequestration. This research provides valuable insights into the geophysical characterization of carbonate reservoirs and contributes to the development of more effective strategies for sustainable

energy production and carbon storage. This research resulted in establishing an approach to estimate in-situ shear wave velocity based on laboratory ultrasonic Vp and Vs and sonic Vp well-log data, thus paving the way for a data driven technique of estimating in-situ Vs , when only sonic Vp is available.

Table of Contents

List of Figures

List of Tables

Acknowledgements

I want to thank my family for their unwavering support. It went a long way in helping me come this far. My deepest gratitude extends to my major advisor and mentor, Dr. Abdelmoneam Raef, whose invaluable guidance and insight were pivotal to this research. I am also indebted to my committee members, Drs. Claudia Adam and Behzad Ghanbarian, for their helpful input, which significantly shaped this work.

Thank you, George, you inspire me always to go for gold.

Lastly to my friends I met in Geology Department, African Students Union and K state at large, thank you all for the friendship. You made my stay here enjoyable.

Dedication

I dedicate this to my future husband and kids.

Chapter 1 - Introduction

Accurate reservoir characterization is a pivotal stage in the development, monitoring, and management of a reservoir, as well as in optimizing production (Aminzadeh & Dasgupta, 2013). The primary objectives of reservoir characterization include identifying the presence of hydrocarbons, assessing reservoir porosity, planning cost-effective recovery mechanisms, and evaluating reservoir permeability. This is accomplished by correlating the petrophysical properties determined by various techniques (core analysis, well-logging, and well-production data) to geologic fabrics (Lucia et al., 2003). Also, this process helps reduce the risk of blow out, inefficient recovery process, and drilling a dry hole.

Previously, researchers noted that fifty percent of oil within carbonate reservoirs, susceptible to waterflooding, remained trapped. Due to extreme geological and petrophysical heterogeneities, the use of basic reservoir models and simulators to stimulate performance faced challenges (Lucia et al., 2003). Geoscientists correlate acoustic and elastic impedance, assess tuning thickness, frequency attributes, amplitude versus offset (AVO), and other seismic indicators to determine crucial reservoir characteristics such as porosity, bed thickness, and potentially, saturation, reservoir pressure, and permeability (Aminzadeh & Dasgupta, 2013). Integrating 3D seismic data with well logs and core analysis facilitates the robust estimation of reservoir volumetrics, fluid properties, and lithology. Seismic data can serve as a bridge connecting well and core analyses.

Geomechanical properties are the physical characteristics of the rock that describe how it behaves under stress including its strength, stiffness and deformation. Geomechanical properties are important because they have direct bearing on drilling including horizontal well drilling, the placement of wells, reservoir productivity and safety with regards to the hydraulic fracturing process. These properties can be obtained either through the laboratory (triaxial/uniaxial tests) or they can be estimated from wireline measurement of acoustic velocities and rock densities (Yale, 1994). Some properties we considered are Young's modulus, Poisson's ratio, Shear modulus and Bulk modulus. Measuring these helps us determine fluid mobility and fluid distribution and this is important for the field being considered for EOR and Carbon sequestration. Bulk modulus helps to predict fluid content because it describes the resistance of a rock to compression, and this depends on the type and amount of fluid in the pore spaces. Young modulus describes the stiffness of a rock while Poisson's ratio describes how rocks react to stress, and this is important to ensure the rocks do not cave in during the execution of the desired project. Shear stress is a force that induces deformation in a material by causing slippage along planes parallel to the applied stress.

Carbon dioxide (CO_2) is a significant greenhouse gas contributing to climate change and its associated challenges, including global warming, droughts, and flooding. To mitigate climate change, there is the need for carbon sequestration. Carbon sequestration is the process of capturing and storing atmospheric carbon dioxide (U.S. Geological Survey, 2025). There are different ways of doing this which include direct capture, biological processes, soil and geological techniques. Our focus is on the geological method which involves storing CO_2 deep underground in porous rock formations. Injecting supercritical CO_2 into geological formations alters the physical and chemical conditions of the subsurface. Both the reservoir rock and the overlying caprock can undergo changes in pore fluid pressure, temperature, chemical reactivity, and stress distribution. These changes may lead to mechanical deformation, the opening or closure of existing fractures (seismicity), and the formation of new fractures (Newell, 2019). Such processes can significantly impact the long-term integrity of geological carbon storage systems, which must remain stable for thousands of years to ensure effective carbon sequestration, and that is why there is the need to understand the physical and geomechanical properties of the rocks.

Seismic attenuation, which is examined at ultrasonic frequency in this project (625khz-20Mhz), is the decay of amplitude of the seismic waves as they move through the subsurface. Propagating seismic waves loose energy due to geometrical spreading, intrinsic attenuation and scattering attenuation. Attenuation is useful to interpret seismic data and laboratory experiments with rocks, and improving the quality and resolution of reflection imaging of the subsurface. In seismology and seismic data processing, a phenomenological quantity called the quality factor (Q) is commonly used to describe these effects (Deng, 2017). Intrinsic wave attenuation has been a topic of research for many years, however most studies examined clastic rocks (Murphy, 1982; Wyllie et al., 1962; Spencer, 1979; Winkler and Nur, 1982). The time lapse variations of attenuation is useful in the seismic monitoring of CO2 injection and storage (Wang & Lawton, 2022) and also evaluating reservoir gas potential (Qi et al., 2017). In the past when there has been studies to measure seismic attenuation, they were performed either in the time domain, such as methods using amplitude decay (McDonal et al. 1958), pulse rise time (Gladwin and Stacey 1974) and wavelet modeling (Jannsen et al., 1985), or in the frequency domain, such as methods of the spectral ratio (e.g., Teng, 1968; Stainsby and Worthington, 1985), the centroid frequency shift (Quan and Harris, 1997) and the peak frequency shift (Zhang and Ulrych, 2002). However, this study seeks to determine the effect of pore fluid on attenuation utilizing laboratory ultrasonic waveform transmission through rock core plugs; dry and impregnated with brine and oil.

1.1 Aims and Objectives

The Mississippian carbonates consist of carbonate reservoirs with significant hydrocarbon reserves (more than 2 billion barrels of oil) (Jaeckel, 2016). The Wellington field is a brown oil field, and there is the need to manage and monitor it to optimize production. This can be done by a better understanding of the geologic complexities in the reservoir to drill wells at appropriate locations to exploit the maximum amount of hydrocarbons, perhaps even beyond what has been estimated. It is also imperative that the reservoir is understood to be able to explore any Enhanced Oil Recovery (EOR) techniques when its quantities are being depleted. The main objectives of this study are the following:

- Determine properties and moduli of the Mississippian carbonates.
- Investigate P-wave and S-wave response to subsurface pore-fluid changes through conducting laboratory fluid replacement methods and laboratory ultrasonic measurements
- Seek integrating laboratory Vs and Vp to deduce Vs at in-situ conditions at boreholes where no dipole-shear logs available. Vs is essential in seismic modeling and fluid replacement studies.

1.2 Previous Study

Ohl & Raef (2014) conducted a comprehensive characterization of the Mississippian formation as a potential site for CO_2-based Enhanced Oil Recovery (EOR) and the underlying Arbuckle saline aquifer for CO_2 geosequestration. Their study utilized a combination of seismic attribute analysis, well log data, and geological information to delineate reservoir characteristics. The coherency attribute was employed to detect anomalous features, potentially indicating lithofacies variations or faulting. Additionally, seismic attributes such as energy, bandwidth, and peakedness of the seismic wavelet were extracted and used to train an Artificial Neural Network (ANN) for lithofacies modeling. Geophysical well logs, including porosity logs, provided key insights into the petrophysical properties of the formation. Cross-plots of well log porosity and acoustic impedance were used to validate the ANN-based petrophysical facies classification. Their research underscored the importance of detailed characterization, particularly of small-scale features, in the effective planning of CO_2 sequestration projects.

Jaeckel (2016) employed an integrated approach using core analysis, thin section analysis, and wireline log data to enhance understanding of the Mississippian formation. Thin section analysis helped quantify grain size, pore types, fossil content, and textural classifications. Wireline logs—including gamma-ray, caliper, neutron porosity, density porosity, and resistivity logs—were used to evaluate the physical properties of the formation. These logs were calibrated with core data to improve facies interpretation and were further used to correlate sequences and cycles within the subsurface. Additionally, porosity and permeability measurements identified reservoir and non-reservoir facies, revealing that the dominant pore types in the Mississippian included moldic, vuggy, and interparticle porosity.

A small-scale field project conducted by Holubnyak (2016) involved drilling, coring, and logging a new injection well (KGS 2-32), with subsequent core and well log analyses that confirmed previously defined flow units and updated geological models. Core plug samples were collected, and relative permeability and capillary pressure curves were derived and correlated with prior estimations for integration into reservoir simulations. Additionally, multiple well tests were conducted, including DST (Drill Stem Test), SRT (Step Rate Test), and interference well tests, which provided valuable insights into permeability, fracture gradient, operational pressures, and well communication within the pilot injection area. Log-derived permeabilities were validated against well test-derived values, while reservoir pressure measurements across five well locations showed a significant decrease from an initial 114 bar to a range of 50–70 psi, emphasizing the need for pressure management in CO_2 injection operations.

Leuck (2017) integrated laboratory-acquired ultrasonic frequency data into fluid replacement modeling, addressing the challenge of accurately obtaining shear wave velocities in carbonate reservoirs. The research utilized saturated elastic moduli and velocities from well logs, alongside dry rock moduli from core plug samples, to evaluate various rock physics models. Among these, the Gassmann fluid substitution model was a primary focus. Comparative analysis revealed a strong correlation between the Gassmann model and Mississippian reservoir data, whereas poorer fits were observed for the Arbuckle formation, indicating that the Gassmann model is better suited for Mississippian carbonates in this context. Additionally, compressional and shear wave velocities (Vp and Vs) measured at ultrasonic frequencies were compared with sonic and dipole sonic log data to assess the accuracy of elastic property estimations at in situ conditions. The study also attempted a Vp-Vs transformation for wells lacking shear sonic logs, but results were inconclusive due to the limited dataset size.

Owusu (2023) advanced reservoir characterization using unsupervised machine learning techniques, specifically K-means clustering and hierarchical analysis, to improve facies delineation and reservoir property prediction. His study also incorporated spectral decomposition and seismic attribute analysis, which enhanced seismic resolution and enabled the identification of subtle geological features. These methodologies provided valuable insights for both EOR and CO_2 sequestration efforts in the Mississippian carbonates.

Building on these prior studies, the present research integrates laboratory ultrasonic velocity measurements with fluid replacement modeling to refine the elastic property characterization of the Mississippian carbonates in Wellington Field, Kansas. By comparing ultrasonic-derived velocities with well log data, this study aims to improve the accuracy of rock physics models for predicting CO_2-induced changes in reservoir properties. The findings will contribute to enhanced reservoir characterization, providing valuable insights for optimizing CO_2-EOR and geosequestration strategies, ultimately supporting more effective reservoir monitoring and injection planning.

Chapter 2 - Geological Setting and Background

2.1 Geologic setting

The Anardako basin has 3 sedimentary sequences (Fritz and Medlock, 1995): 1) Sauk Cambro-Ordovician Arbuckle Group, 2) Tippecanoe Ordovician Viola Group and Siluro-Devonian Hunton Group, and 3) Kaskaskia Mississippian Osage-Meramec-Chester limestone sequence. Of importance to our research is the Kaskaskia Mississippian Osage-Meramec-Chester limestone. The term "Mississippian limestone'' is a term that describes the Mississippian age strata across the mid-continent (Fig. 2.1). Subsurface reservoirs that have been drilled in the Mississippian have their stratigraphy extending from Kinderhookian to Chesterian and have their stratigraphic equivalents in outcrops in Oklahoma, Missouri and Arkansas (Mazullo et al., 2019). The Mississippian is composed of a mixture of carbonate including limestone and dolomite as well as siliciclastic rocks and cherts. The Mississippian carbonates of southern Kansas, where the Wellington field is located, is dominated by siliceous sponge-bearing dolomitic facies including bedded spiculite and silty organic shale (Mazullo et al., 2019). Chert occurs as layers and lenses within the Missisipian rocks of the midcontinent and is predominantly present in Osagean strata. This forms the Chert reservoir which is characterized by high porosity and low permeability and function as excellent reservoirs if fractured (Grammer, et al., 2019).

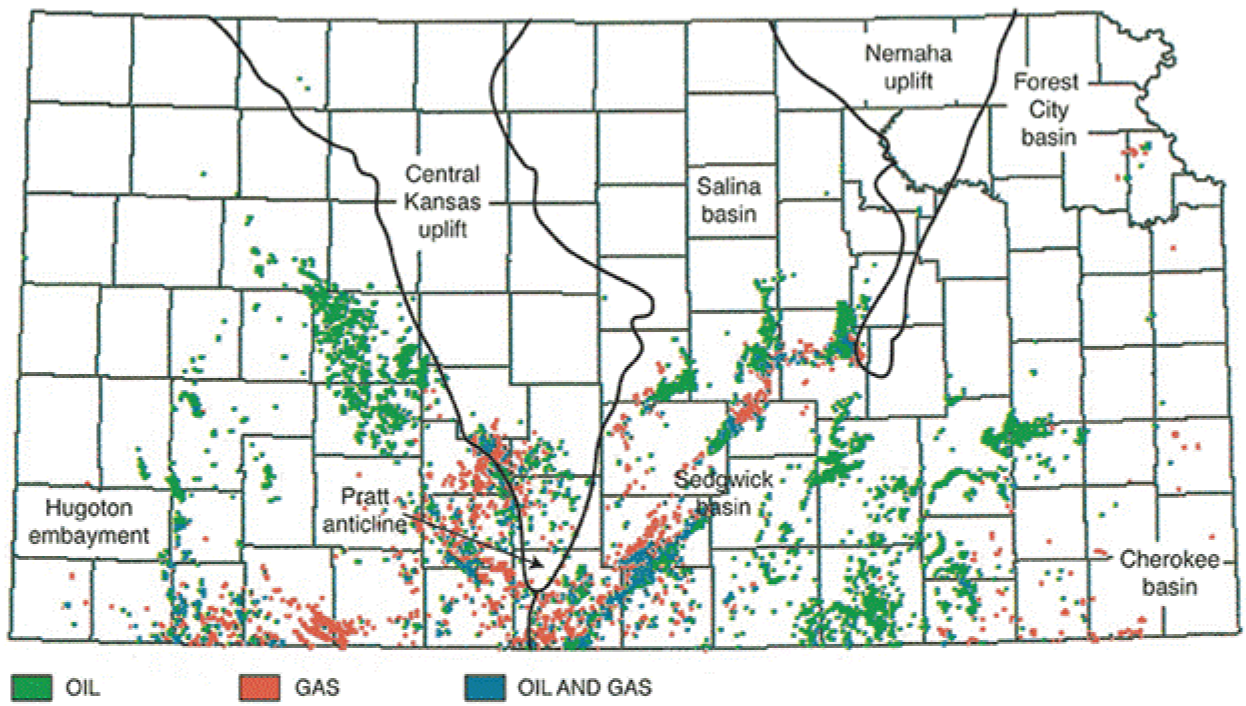

Figure 2.1 Distribution of Mississippian limestone in Kansas(Kansas Geological Survey, 2013).

2.2 Tectonic history

Tectonic events that happened in the early Mississippian age resulted in the pattern of structures represented by the most notably Central Kansas uplift in north western and central Kansas and the Nemaha uplift that began in Eastern Kansas in the late Mississippian. The Central Kansas uplift is a broad complex structural high that trends northwest to southeast across central Kansas (Evans and Newell, 2013). The timing of the development of the Central Kansas Uplift has been debated due to extensive uplift and erosion in Early Pennsylvanian time that led to the removal of most of the older Paleozoic rocks surrounding central Kansas (Adkison, 1972). The Nemaha uplift influenced the spatial distribution of the 'Mississippian Lime'. This is because, during this period several small crustal blocks (horst and graben fault–block pattern) were uplifted and eroded in Late Mississippian and Early Pennsylvanian (Wittman, 2013). An example is the

Nemaha ridge. This feature is a 25-mile wide, transtensional graben with an inverted, horst block core. (McBee, 2003). It is exposed to the surface in southeastern Nebraska and plunges south and slightly west. Hydrocarbon reservoirs are found in the mid-continent because of stratigraphic and structural traps that served as migration pathways along the uplift zone (Dolton and Finn, 1989). The south plunging Pratt anticline is an extension of the Central Kansas uplift lineament, which separates the Sedgwick basin to the east and the Hugoton embayment to the west. During the early to middle Paleozoic, it formed part of the shelf region of the Anadarko Basin (Wittman, 2013) (Fig. 2.2).

A post-Mississippian normal fault, oriented in a NE-SW direction and dipping SE, bisects the Wellington field, dividing it into two sections. This fault extends through the Mississippian and the Arbuckle Group down to the basement. Its formation has resulted in accommodation space above the Mississippian chert reservoir, particularly in the southeastern part of the Wellington field (Fadolalkarem, 2015).

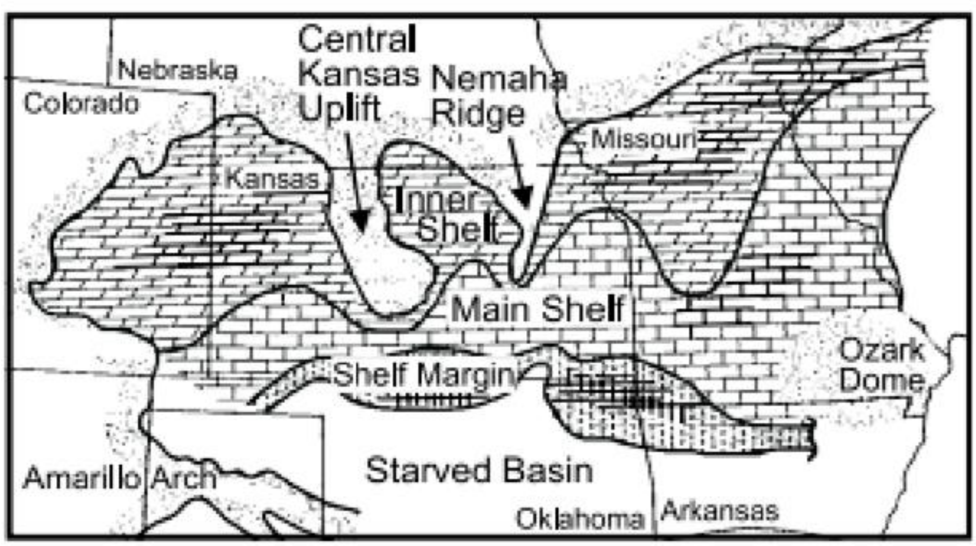

Figure 2.2 Paleographic map of the Midwest, specifically Kansas, and surrounding areas during the Osagean. It displays the shelf margin, basinal conditions, as well as both the upper and lower shelves(Watney et al., 2001).

2.3 Stratigraphy

The stratigraphy of the study area is shown in Fig. 2.3. The Kinderhookian Shale is located at the base of the Mississippian, followed by the Osagean, Meramecian, According to Mazzullo et al., (2019), the depositional geometry is aggradational for the lower Mississippian and progradational for the middle to Upper Mississippian group. The Kinderhook shale is composed of dark gray to green-gray silty shale and limestone. The Bachelor, Compton, and Northview Formations are found within the Kinderhookian section. A glauconitic interval at the bottom of the Pierson marks the base of the Osagean section (Krueger, 1967).

The Osagean strata comprises of low resistivity, high porosity chert-rich formations (‘chat’), the most prolific hydrocarbon reservoirs in south-central Kansas (Watney et al., 2001). Both conventional and unconventional Mississippian reservoirs in the mid-continent are made up of chert-rich carbonates of Osagean and Meramecian age (Cahill, 2014).

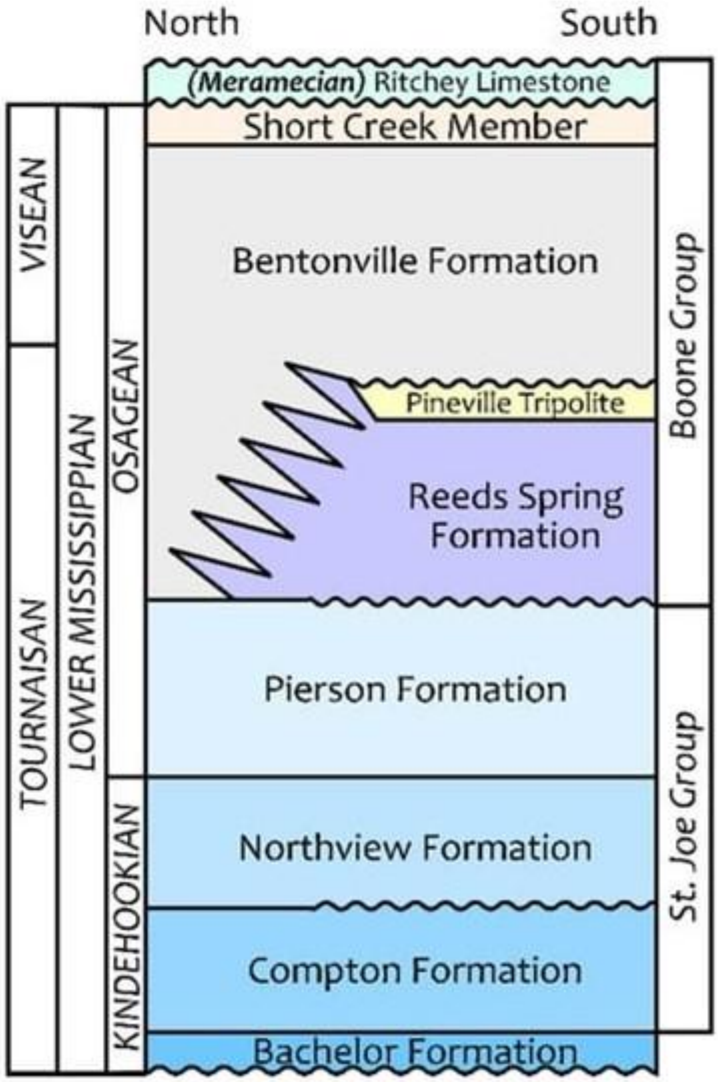

Figure 2.3 Stratigraphy of the study area, modified after Okyay et al., (2016).

2.3 Porosity

The primary grain type consists of sponge spicules and their molds, embedded within a dolomite mudstone matrix. Porosity is predominantly moldic, intercrystalline, and intergranular, with a notable presence of vugs. In certain areas, subaerial exposure and karstification have led to the formation of fenestral and vuggy porosity. Porosity tends to be highest in grainstones and lowest in mudstones. The grain and crystal sizes are fine, ranging from less than 100 μm to below 2 μm, leading to the development of extremely fine microcrystalline pores (Guy et al., 1999).

The porosity of Mississippian rocks in this region has been significantly impacted by a series of diagenetic events, including fracturing, dissolution, and cementation (Young, 2010; Wojcik et al., 1992). Specifically, King (2013) found nine such events in the KGS 1-32 core, demonstrating the complex diagenetic history and its influence on porosity. Brecciation, fracturing, and carbonate replacement with microporous chert are common in all lithologies, contributing to secondary porosity through fracture networks and microporosity within the chert matrix. Fracturing and the presence of vugs contribute to increased permeability at any location. Helium porosity values measured on core plugs range from 4% to 26%. Vuggy porosity in mudstones appears to be isolated, whereas in wackestones, it exhibits better connectivity (Carr et al., 1998).

2.4 Hydrocarbon Production

Kansas is a well-established petroleum-producing region with numerous oil and gas fields managed by over 3,000 independent operators. Due to operational challenges and depositional-diagenetic variations, most fields achieve recovery efficiencies below 30% of the original oil in place (OOIP), leaving substantial remaining oil in place (ROIP). By utilizing enhanced oil recovery methods, operators can tap into these remaining reserves, enhancing recovery efficiency and maximizing production from existing fields.

Oil from a Mississippian reservoir was first produced in 1904 in Osage County, Oklahoma (S &P Global, 2016). The Wellington oil field, producing from the Mississippian and Arbuckle formations since 1929 has yielded over 20 million barrels of oil. Currently, Berexco LLC operates

55 active wells within the field (Holubnyak et al., 2017). Figure 2.4 shows the fraction of oil being recovered from the Mississippian compared to other formations.

In the Lower-Middle Mississippian strata, hydrocarbon production occurs from carbonates, cherty carbonates, and chert-rich formations primarily composed of heterozoan-dominated carbonate biota and biosiliceous material (Franseen, 2006).

Increasing oil prices, combined with the advancement of horizontal drilling technology initiated a new era of Mississippian reservoir development in the early 21st century (Wilson et al., 2019). Mississippian production in Kansas and Oklahoma reached its peak in 2015, producing nearly 500,000 barrels of oil and close to four billion cubic feet of gas per day (S &P Global, 2016). As of 2024, the Wellington field, where our focus is, has produced 21,096,233 cumulative barrels and 50 wells have been drilled. (Kansas Geological Survey, 2025)

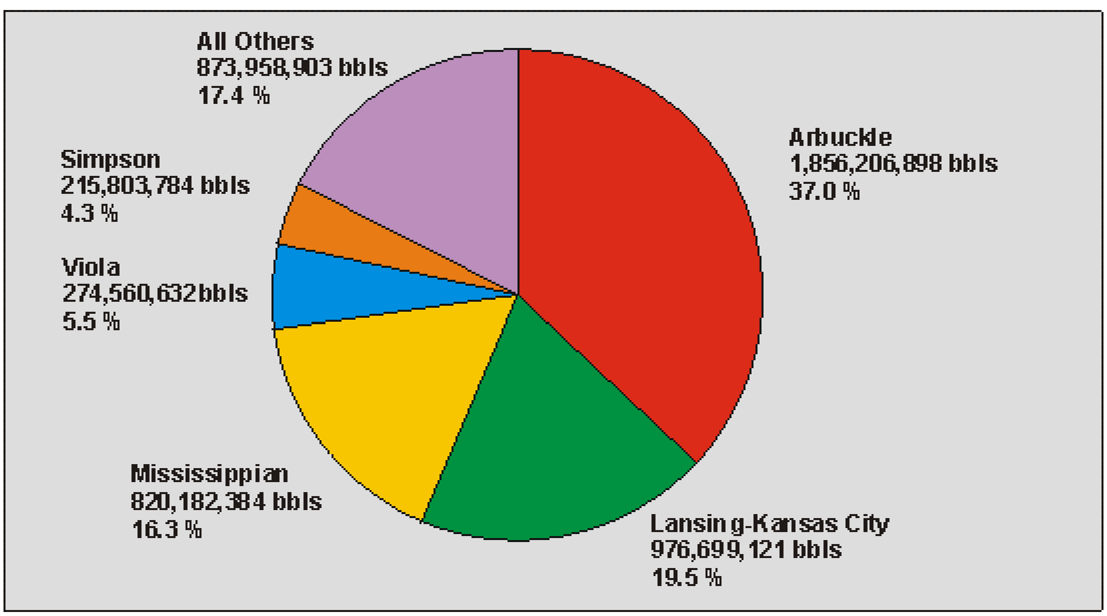

Figure 2.4 Oil production by geologic units in Kansas since 1970 (based on production numbers from the Kansas Geological Survey).

Chapter 3 - Data and Methods

To characterize reservoir rocks, we need to understand the elastic properties of the rocks. These refer to the elastic moduli which determine Vp and Vs velocities. The values for the velocities were obtained by taking laboratory ultrasonic measurements using Ultrasonic in-house pulse transmission laboratory setup.

Ultrasonic velocity measurement for determining the elastic properties

Ultrasonic wave measurements serve as sensitive indicators of subtle geological processes that are challenging to observe directly, such as variations in porosity, contact stiffness, and the formation of foliation and shear fabric. The elastic properties of rocks are primarily controlled by the solid rock framework, including structural defects such as pores, fractures, and cracks. Compressional wave velocity (Vp) is controlled by the type of pore fluid (gas, liquid). Shear wave velocity (Vs) is not strongly controlled by the type of pore fluid. A combination of both these data help to determine elastic moduli:

Young Modulus

The Young's Modulus (E), in equation 1 measures rock stiffness; a larger E value signifies a rock's resistance to deformation. This resistance directly impacts fracture width: stiffer rocks (high E) produce narrower fractures, while less stiff rocks (low E) result in wider fractures

$$E=\frac{pV_s^2(3V_p^2-4v_s^2)}{V_p^2-V_s^2} \qquad (1)$$

Poisson’s ratio (σ)

Poisson's ratio, (equation 2) defines how a material deforms in perpendicular directions. Since compressional and shear waves generate deformations at right angles, Poisson's ratio helps understand their interdependence. Specifically, it measures the ratio of lateral contraction to axial extension, offering a crucial metric for evaluating a material's elastic properties

$$\sigma = \left(\frac{Vp^2 - 2Vs^2}{2(Vp^2 - Vs^2}\right) \quad (2)$$

<u>Shear modulus</u>

The shear modulus, (equation 3) is a key property that quantifies a material's resistance to shearing deformation. Materials that are more resistant to shear will transmit shear waves at a faster rate. This resistance is measured by calculating the ratio of shear stress to the tangent of the resulting deformation angle.

$$\mu = \rho * Vs^2 \quad (3)$$

<u>Bulk modulus</u>

Bulk modulus (equation 4) is defined as the proportion of volumetric stress related to the volumetric strain of specified material while the material deformation is within elastic limit.

$$k = \frac{p(V_p^2 - 4V_s^2)}{3} \quad (4)$$

3.1 GCTS ULT 100 Ultrasonic Velocity Test System

The ultrasonic elastic properties of rock samples can be assessed using several well-established industry techniques, including pulse transmission, pulse echo, and resonant ultrasound spectroscopy methods. In this study, we utilized the pulse transmission method, an approach widely used for measuring the dynamic elastic properties of rocks, as done by Birch (1961) and Bakhorji (2010). The pulse transmission method is a non-destructive method that involves measuring the time it takes for a pulse to pass through a rock and calculating ultrasonic velocity by dividing a known distance by the measured time.

The ULT Ultrasonic Velocity system manufactured by GCTS Testing Systems (Fig. 3.1) is comprised of a ULT 100 controller, 2 platens and a Graphical User Interface called Cats Ultrasonic Software which is installed on any computer. The software is responsible for giving users interaction with the controller and conducting experiments. The ULT 100 controller runs the program, controls the pulse, performs tests and reads and saves files. The controller can only be accessed through the software.

The experiment was run with Cats Ultrasonic 1.81 Software installed on a Windows computer, the controller box, the 2 platens served as the source and receiver transducers. The transducers are made up of piezoelectric ceramics, a polarized material that transforms an electrical pulse into mechanical vibrations in source mode and converts mechanical vibrations into electrical signals in receiver mode.

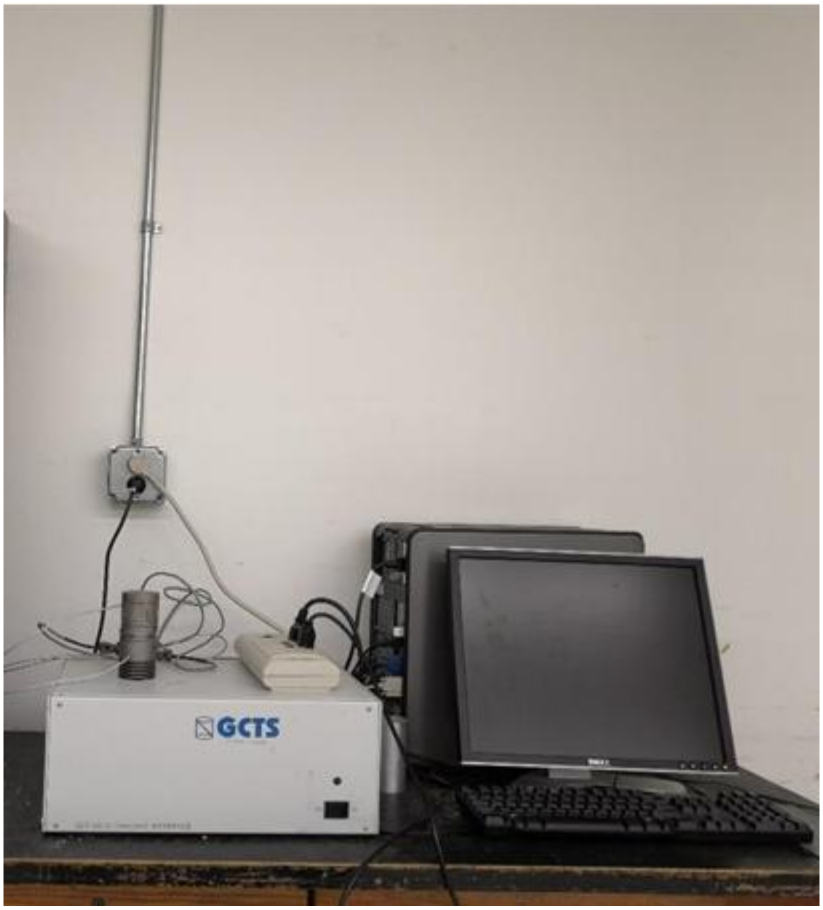

Figure 3.1 GCTS controller system with the 2 platens and the computer on which the software is installed.

A hydraulic press by Carver Inc served as overburden pressure (Fig. 3.2). The lab setup was the same as that of Shodunke (2021). The ultrasonic velocity system can be used to calculate Compressional wave velocity (Vp) and shear wave velocity (Vs) digitally or manually. This is done by locating ‘first arrival time’ of the wave. First arrival time is the time it takes a wave to travel through a sample and be recorded. This can also be done automatically by the software or can be decided manually by a person. Manually, it can be found at the exact time at which either the P wave or the S wave pulse begins to form, just after the noise.

Figure 3.2 Carver hydraulic press that exerts pressure.

The ultrasonic test was conducted on core side plugs from the Mississippian in the Wellington field, obtained from Kansas Geological Survey. There were 12 samples in total, taken between depths of 3658 to 4100ft of the KGS 1-32 well, which is the depth of the Mississippian (Fig. 3.3). Each sample had a length of 7 cm and diameter of 2.5 cm. The rocks were obtained dry so there was no need to oven dry them before proceeding. They were checked for cracks which will lead to reduced velocity measurement, as a result of increased travel time, however they were all found to be very good samples. Next, their lengths, diameter and weight were taken with the help of a rule, caliper and a scale (Fig. 3.4).

Figure 3.3 Well labeled carbonate rock core-plugs samples from the Mississippian.

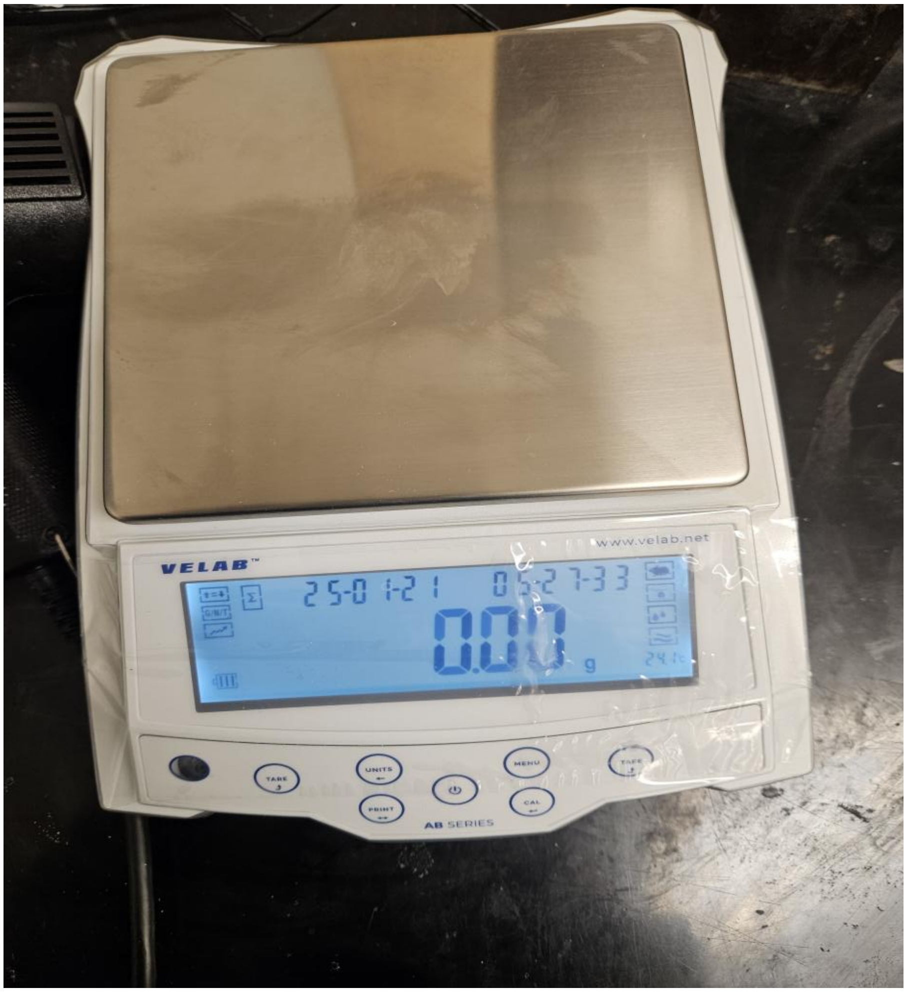

Figure 3.4 Scale used to take weight of samples.

An initial platen to platen (face-to-face test) (Fig. 3.5) is run where no sample except a couplant (honey) is used to stick the platens together and an ultrasonic frequency pulse generated to run through them. This is done to determine the face-to-face time it takes the ultrasonic frequency pulse to travel through the platens only and also to ensure a reliable signal is being obtained. This face-to-face time arrival time is subtracted from all the subsequent arrival times of cores, since that was the time taken for the pulse to get to the platens and not the cores directly.

Figure 3.5 Face to face of platens (left). Honey used on platens to ensure good coupling (right).

To ensure we were getting accurate results, we had a test run, where we used an aluminum core, since the velocity of aluminum was provided in the software manual (Fig. 3.6). The length and time it took the ultrasonic frequency pulse to travel through the aluminum core was taken and divided to find the measured ultrasonic P and S velocity and compared to the known velocity. The values were confirmed to be accurate.

Figure 3.6 Velocity measurements being taken on aluminum core.

We then conducted our experiment on our cores. All our cores were checked and ensured they had flat ends to allow wave forms to allow good coupling which is required for ultrasonic wave forms to be transmitted from transducers to cores and also allow cores to be placed steadily on transducers. Those that were not perfectly flat were flattened using a water-cooling electric saw. Establishing an acoustic connection between the transducers and the rock sample is essential, which is why honey was used. Additionally, honey serves as a coupling medium, facilitating the transmission of ultrasonic energy from the transducer to the rock. It was important that air gaps are not between the transducers and the rock sample since this will produce a weak signal or will not allow P and S waves to pass through. Honey was specifically chosen because of its low viscosity as well as its ability to not interact with the minerals in the rock.

Before P and S wave velocities could be calculated, the software required that some inputs be entered, such as the type of platens used (NX was used for all core samples), type of rock, height of sample in millimeters, weight in grams, and diameter in millimeters, and these were used to calculate the density of the rock which was needed in calculating the velocities (Fig. 3.7). Frequency of sampling rate also had to be chosen and we used 156 kHz, 312.5 kHz, 625 kHz, 1.25MHz, 2.5MHz, 5 MHz, 10 MHz and 20 MHz for the experiments because we wanted to understand how frequency impacts velocity. Other configurations that were required were External manual gain (which was turned off for all experiments), Energy output percent (kept at 100) and input automatic gain (kept at 20).

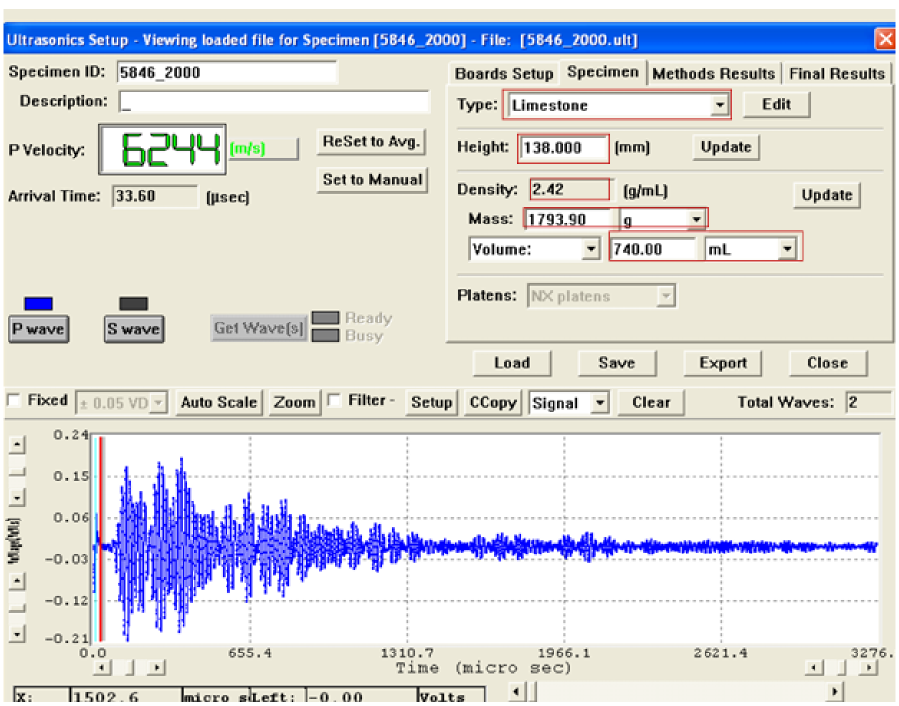

Figure 3.7 GCTS ultrasonic software configuration interface displaying input parameters and data required for generating and capturing ultrasonic waveforms(GCTS Testing Systems)

Once the rock is placed between the platens and pressure is applied, the P and S wave signal buttons on the software are clicked and waves are sent through the rock. The automatic method of determination by the software was first used. This method provided a first arrival time, P and S wave velocities, as well as elastic moduli like Poisson's ratio, Young's modulus, Bulk modulus and shear modulus.

However, this method of determining the velocities was realized to be inaccurate since the first arrival times picked by the software were further away from the first wave that was seen after the noise. Hence, a different method was utilized. For each sample at a constant pressure of less than 10000lbf, all the 8 frequencies (156 kHz, 312.5 kHz, 625 kHz, 1.25 MHz, 2.5 MHz, 5 MHz, 10 MHz and 20 MHz) were used successively. After clicking the P and S wave button to obtain the waveform, P and S wave data was exported to Microsoft excel where Raw signal (y axis) against time (x axis) was plotted on a graph. For a given rock sample, graphs of Raw signal and time of each frequency were superimposed on one another in order to determine the exact location of the first arrival time, which was observed to be the time at which the first sinusoidal wave starts just after the noise. It was hard to determine exactly where first arrival starts, hence just like Cimino (2020) and Shodunke (2021), the time was picked from where the waves started separating (Fig. 3.8). That time was converted from millisecond to second and divided by the length of every sample to determine velocity.

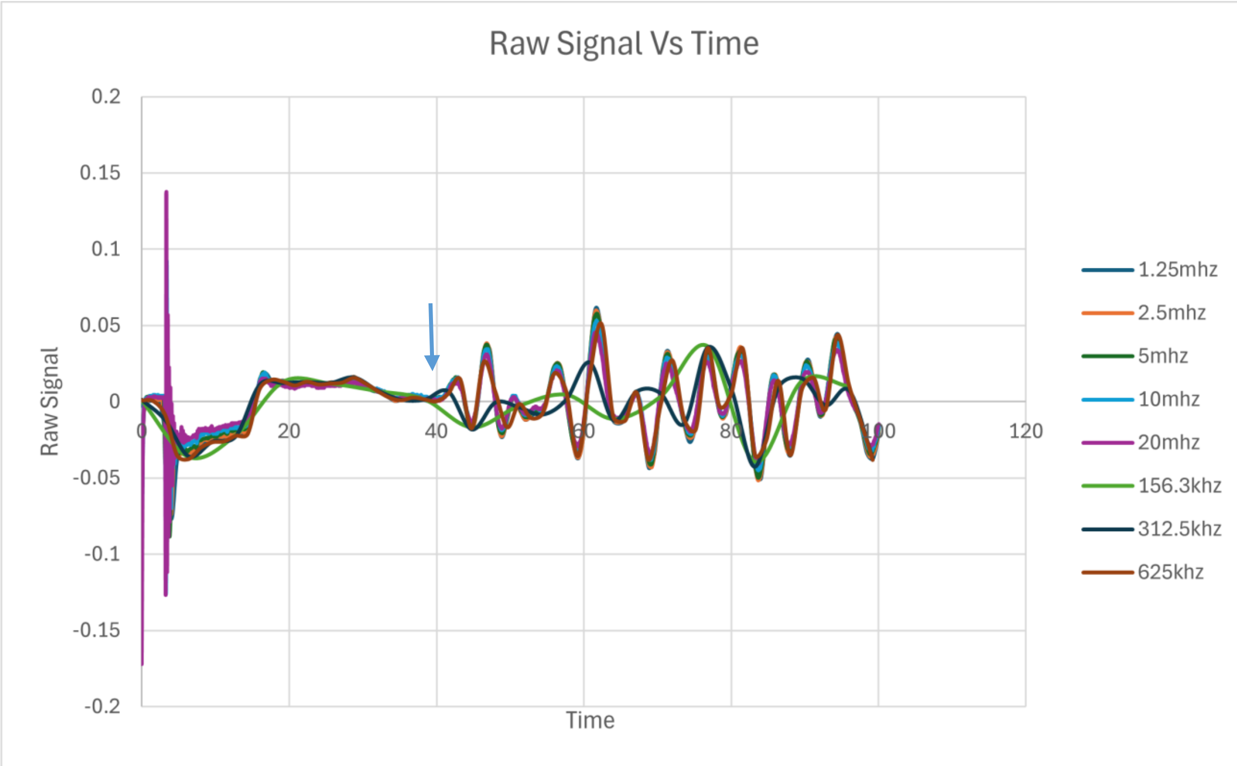

Figure 3.8 First arrival time being determined for a sample.

3.2 Fluid Substitution Modeling

The fluid substitution modeling technique is a crucial tool that allows the prediction of the elastic response of a rock saturated with one type of fluid based on the elastic response of the same rock saturated with another fluid (Akpan et al., 2020). The introduction of fluid substitution modeling in seismic reservoir characterization has notably propelled breakthroughs in the exploration of oil and gas (Akpan et al., 2020). Fluid substitution modelling allows us to obtain and observe various seismic responses to different formation fluids as well as fluid saturation in the reservoir pores. It provides the interpreter with different fluid scenarios which will produce different Amplitude vs Offset (AVO) responses.

Many models can be used for fluid substitution modelling including Gassman's modelling (Gassmann 1951), Patchy (Mavko et al., 2009), Biot & Gassmann modelling (Mavko et al., 2009), etc. Gassmann fluid replacement modelling is the most widely used method because the input parameters are straightforward and can be obtained from logs. (https://petrowiki.spe.org/Gassmann's_equation_for_fluid_substitution). The assumptions according to Xu & Payne (2009), Wang (2010), Smith et al. (2003), Adam et al. (2006), Wang and Nur (1992), and Simm and Bacon (2014) of this model are as follows;

1. Porous material is isotropic, elastic, monomineralic, and homogeneous
2. Pore space is well connected and in pressure equilibrium (zero frequency limit)
3. Medium is a closed system with no pore fluid movement across boundaries
4. No chemical interaction between fluids and rock frame

This is not so for our area of interest since we are dealing with carbonates who have undergone diagenesis and porosity is not homogenous. Another shortfall about this method is that the densities, bulk moduli, velocities, and viscosities of common pore fluids are over simplified.

The Gassmann's model (Gassmann 1951), which is commonly used in petroleum rock physics is suitable for rocks with spherical and interconnected pores at low frequencies. These assumptions do not necessarily meet the conditions of carbonate rocks as well as the frequencies used in this experiment. Since in most carbonate rocks many isolated pores exist, Gassmann’s assumptions are not necessarily valid (Adam et al., 2006).

3.2.1 Fluid substitution Experiment

The goal is to test for how velocity of rocks varies with each fluid contained in it. We sought to have a proxy of the fluids in the subsurface and so we used brine, mineral oil and a mix of both brine and mineral oil saturation. At room temperature of 20˚C/ 68˚F, 357 g of NaCl is needed to saturate 1 liter of water. However, after measuring 1000 ml of water and measuring 357 g of NaCl, and adding it to dissolve, it did not. It was stirred for a few minutes and since it appeared to be too concentrated, we added another liter of water, and it completely dissolved. Dry rock samples were weighed and immersed into the prepared brine fluid in the desiccator. The vacuum pump was connected and was used to ensure there was no air in any pore space of the rock, i.e. it sucked the air in the pore spaces, thus creating a vacuum all the pore spaces are filled with whatever fluid was in the desiccator (Fig. 3.9).

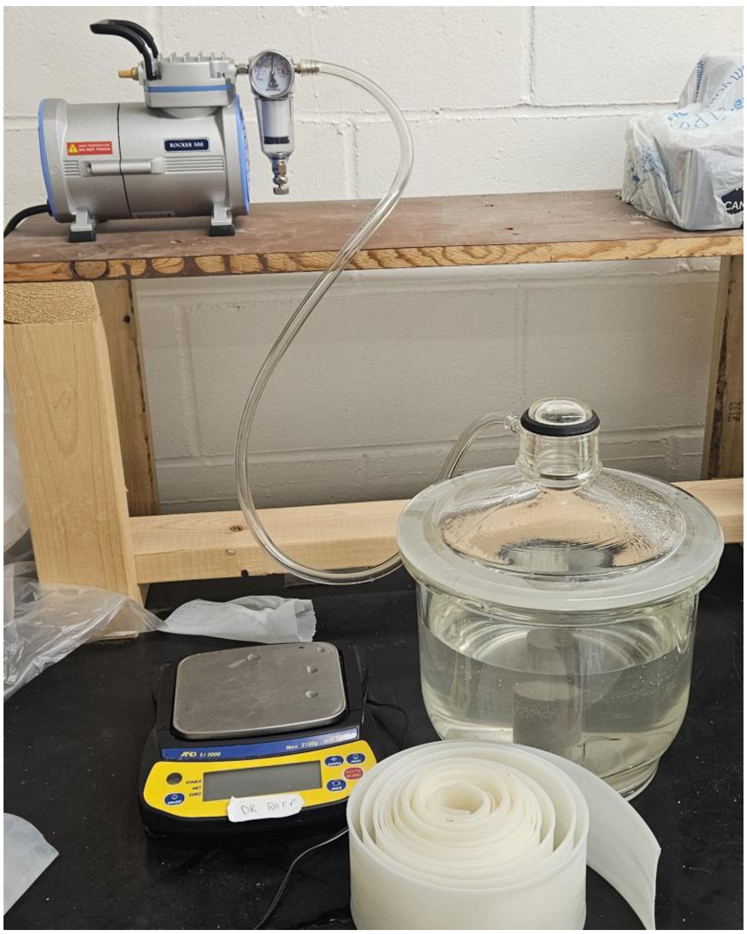

Figure 3.9 Desiccator containing sample saturating brine and vacuum pump at the top.

Brine was the first fluid put in the desiccator, then saturation was done, and brine was replaced with mineral oil to saturate the rocks. Mineral oil was used because it has very similar properties to the oil found in the subsurface and does not stain the rocks. Full saturation of brine was first done. To confirm if the rock was completely saturated, the bubbles coming from the rock in the desiccator were observed-no bubbles from the rock gave the indication that the rocks were completely saturated with the fluid (Fig. 3.10).

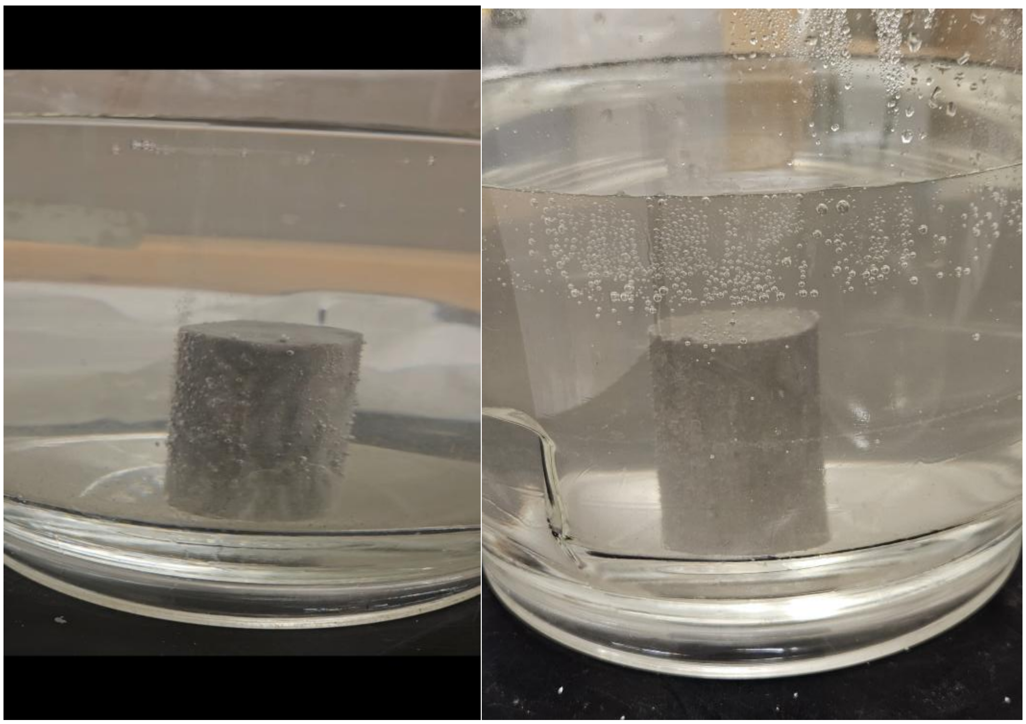

Figure 3.10 Close up of sample undergoing saturation with bubbles coming out(left). Sample after saturation with no bubbles from the sample (right).

They were taken out and re-weighed, and then velocity measurements were taken. The samples were air dried to allow some brine to move out, since we wanted to perform partial saturation of brine and oil. The samples were constantly weighed to ensure that half the volume of water remained in the rock sample to be able to proceed with the partial saturation in oil. E.g. if a sample weighed 185.6 g when dried and weighed 187.1 g when fully saturated with brine, weight of brine is 1.5 g and so getting a partial saturation of water means it should weigh approximately

185.6+0.75=186.35 g before it could be immersed into oil. Samples that got dried below the amount or were completely drained of their water (this was known using the weight of the samples when dry) had to be partially saturated with brine again before being put in oil. During the partial saturation process, samples were taken from the desiccator, weighed on the beam balance and compared with the weight the sample is supposed to have when completely saturated. This ensured the sample was saturated with both oil and brine and it had no pore space. Then velocity measurements were carried out. The samples had to be air dried again to ensure the brine had dried out and only oil had filled the pores. It was immersed into the desiccator which had oil to completely get saturated with oil. Again, the samples were weighed at short intervals to ensure the expected weight at complete saturation was achieved. After being fully saturated with oil, velocity measurements were again taken using the ULT 100 ultrasonic velocity instrument, at all 8 frequencies. All velocity data of samples in their different stages of saturations were exported to excel. 12 samples were used for the dry rock experiment, but 4 samples broke due to excess pressure and so 8 samples were used for the brine saturation experiment. After this, 3 other samples got fractured, leaving us with 5 samples for the oil saturation.

3.3 Velocity Determination and Comparison

The ultrasonic velocity of each sample was determined by dividing the sample length by the first arrival time corrected by the subtraction of the face-to-face time (Table 3.1) unlike the automatic determination using the Ultrasonic system as done by Lueck (2017), Cimino (2020) and Shodunke (2021).

3734.2	Freq	P wave	Time (us)	Time (s)	Velocity(P)	S wave	Time (us)	Time (s)	Velocity(S)
	10	39.2	12	0.000012	5833.3	40.8	26.8	0.0000268	2611.9
	1.25	36.8	9.6	0.0000092	7291.7	42.4	28.4	0.0000284	2464.8
	2.5	42.4	15.2	0.0000152	4605.3	42.8	28.8	0.0000288	2430.6
	5	40.4	13.2	0.0000132	5303.0	42.6	28.6	0.0000286	2447.6
	20	41.05	13.85	0.00001385	5054.2	42.15	28.15	0.00002815	2486.7
	156.3	38.4	11.2	0.0000112	6250.0	44.8	30.8	0.0000308	2272.7
	312.5	38.4	11.2	0.0000112	6250.0	44.8	30.8	0.0000308	2272.7
	625	38.4	11.2	0.0000112	6250.0	44.8	27.6	0.0000276	2536.2

Table 3.1 Velocity calculated from first arrival time and length of sample for each frequency.

Sonic Vp and Vs (unit in microseconds per feet) was acquired from seismic data for all 5 samples and converted to velocity (unit in meter per second). Both ultrasonic and sonic velocities were compared. Poisson's ratio ultrasonic velocities for each frequency was calculated using $(Vp^2-2Vs^2)/2(Vp^2-Vs^2)$.

Sample	Freq	Sonic Vp	Ultrasonic Vp	Sonic Vs	Ultrasonic Vs	Vp^2	Vs^2	Poisson's ratio
	10	5025.5	4565.2	2942.5	2210.5	20841051	4886310.25	0.346869645
	5		4565.2		2218.3	20841051	4920854.89	0.345452433071
	20		4500		2202.8	20250000	4852327.84	0.342433071

	2.5		4500		2187.5	20250000	478156.25	0.345289214
	1.25		4632.4		2218.3	21459129.8	4920854.89	0.351228289
	156.3		5625		2045.5	31640625	4184070.25	0.423805621
	312.5		5625		2282.6	31640625	5210262.76	0.40143414
	625		4375		2157.5	19140625	4654806.25	0.339332304
								Average= 0.361980591

Table 3.2 Poisson's ratio.

Since Poisson’s data is unitless, we used it for comparison. We calculated the average of Poisson’s data and tried to work it backwards to get Vs and compare it to the Vs provided by seismic data (Table 3.2). We observed a small margin of about 600m/s and it was due to overburden pressure. Whereas the subsurface has overburden rocks which exert pressure, our laboratory experiment was controlled and so did not have as much pressure, hence that impacted Poisson’s ratio.

3.4 Porosity

Porosity refers to the ratio of pore volume to the total volume of a rock or material, typically expressed as a percentage. It is calculated as a fraction or as a percentage, indicating the proportion of pore space and fracture space within the rock type investigated. Porosity is a crucial parameter for estimating in-place reserves in the exploration and production of hydrocarbon oil and gas. Porosity is expressed as: $\phi = V_v/V_T$

Where ϕ = Porosity, V_v = Void volume, V_T= Total volume

Some porosity measurement methods include a direct method using core samples. Optical methods using visual inspection and image analysis, imbibition methods, gas expansion, water evaporation, and thermoporometry.

<u>Fluid displacement Method</u>

To find the porosity using weight displacement, the mass of the dry rock was measured and immersed in an impregnation fluid of known density. The rocks were left in the fluid overnight to allow for maximum saturation. The weight difference corresponds to the volume of fluid occupying the pore spaces, which is then used to determine porosity by dividing the pore volume by the total rock volume. Using the Archimedes principle, the volume of fluid displaced is equal to volume of water displaced. Hence to find the total rock volume, it was immersed into a known volume of fluid. The increase in volume is equal to the total volume of the rock.

<u>Porosimeter</u>

A porosimeter measures the amount of pore space within a rock sample to determine its porosity. This is essential for assessing the rock's ability to store and transmit fluids such as water, oil, or gas. The porosimeter analyzes the pore size distribution and assesses the permeability of a rock sample by measuring the volume of fluid that can be injected into its pores under controlled pressure.

The Helium Porosimeter is a compact benchtop unit designed for precise porosity measurements. It includes a sample chamber, reference volume, isolation valves, a high-precision pressure transducer with a digital display, and a thermocouple for accurate temperature readings. The system also features a gas connection manifold, compatible with helium or other gases like mercury (in this case we used Helium), along with a set of precision spacers for enhanced measurement accuracy. The system requires one electrical connection, a regulated Helium pressure supply, and a computer with a USB port since the software is provided on a USB. Helium is the gas preferred for Boyle's law porosimetry because helium is non adsorbing and also has little deviation in behavior. The size of the helium molecule is small, and thus the helium method of determining porosity provides an approximate estimate of the total porosity (Kelley & Saulnier, 1990). Helium Porosimeters function based on the principle that the pressure of an ideal gas in a confined space is related to the chamber's volume. By accurately measuring the volumes of two pressure vessels—the reference volume and the sample chamber—the grain volume of a solid sample can be determined. This is achieved by analyzing the pressure change when the pressurized reference volume is connected to the sample chamber.

Samples are first measured to determine their length and diameter in inches. To begin the test, the sample chamber was isolated from the reference volume by positioning the left valve upward toward "VENT." The sample was placed inside the chamber along with the provided precision spacers. The type of spacers used was dependent on the shape and length of the samples. The goal was to use spacers that will be enough to allow the cap to be tightly closed and have the mark facing a 12 o'clock. The spacers (Fig. 3.11) were used to ensure precise and accurate measurements. The selected spacers were chosen in the software as well as the diameter and length of each sample (Fig. 3.12).

Figure 3.11 Spacers used in porosimeter.

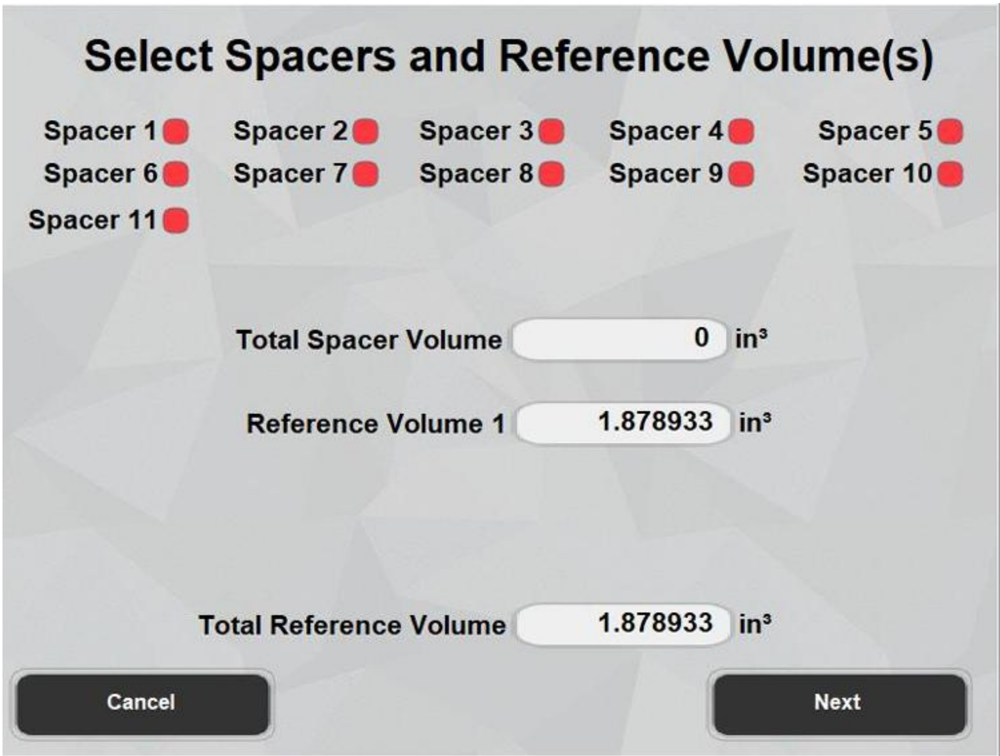

Figure 3.12 Spacers are selected according to the ones used for a specific sample.

With the porosimeter connected to an external source of helium regulated to the maximum pressure of the porosimeter, the “INLET” valve was opened to allow the gas into the system while still isolating it from the sample with the left valve. It should be noted that the pressure cannot exceed 110 else the transducer will be damaged. Once it reached about 100-105, the “INLET” valve was turned to isolate the reference volume from the Helium source. Next, the “VENT” valve was used to connect the reference volume to the chamber volume ie where the sample was, allowing gas to expand into the sample chamber. This is done by placing the left valve in the 6 o’clock direction. After pressure has stabilized and equilibrium is reached, the final readings can be taken. That is, helium was used to pressurize the reference volume. Once pressure and temperature stabilized, the initial pressure was recorded using the provided software. The isolation valve was then opened, allowing gas to expand into the sample chamber. After equilibrium is reached, the new pressure is recorded, allowing for the calculation of pore volume and porosity (Fig. 3.13) The software also provides options to view and print reports for multiple samples.

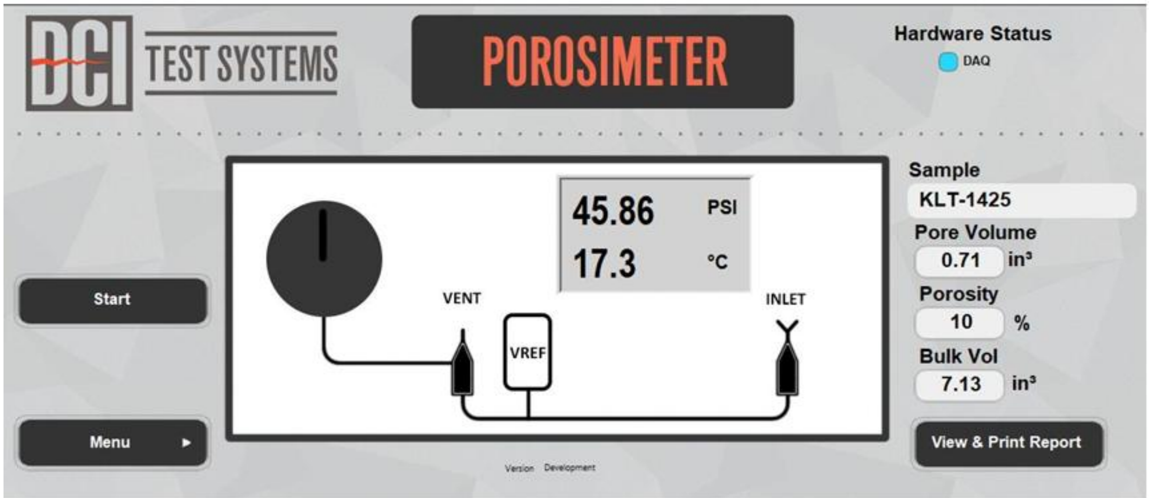

Figure 3.13 Porosity values are displayed by the software.

Wyllie time-average equation

Wyllie et al. (1958) established an empirical relationship between velocity and porosity that aligns well with data from well-consolidated sandstones and limestones. This relationship, known as the Wyllie time-average equation (Wyllie et al., 1956), is based on intuition rather than fundamental physical principles. Accurately evaluating the porosity of a clean formation requires consideration of the matrix type and its characteristics. A strong correlation is often observed between porosity and acoustic interval travel time, making this equation a widely used tool in formation evaluation.

Φ_s=Δt-Δtma/Δtf-Δtma (5)

Where Δt is the sonic transit time (As/ft), Δtma is the sonic transit time of the matrix (As/ft), Δtf is the sonic transit time of the fluid (As/ft), and ϕ_s is the sonic derived porosity (PU or %).

This equation, (equation 5) which links acoustic travel time to matrix and fluid travel times, is widely applied to quantify sonic porosity in consolidated sandstones and carbonates with intergranular porosity.

	V_{ma} (ft/s)	Δ_{tma} (µs/ft)	Δ_{tma} (µs/ft) (Commonly used)
Sandstone	18,000–19,500	55.5–51.0	55.5–51.0
Limestone	21,000–23,000	47.6–43.5	47.6
Dolomite	23,000–26,000	43.5–38.5	43.5
Anhydrite	20,000	50.0	50.0
Salt	15,000	57.0	67

Table 3.3 Some constants used in the sonic porosity formula (Schlumberger, 1972).

Spikes and Dvorkin (2005) observed that the Wyllie time-average equation is inconsistent with Gassmann's (1951) fluid substitution equation. As a result, the time-average equation is typically applied only when brine is used as the saturating fluid.

Since our samples were limestone, we used sonic transit time of matrix for limestone which is 47.6 µs/ft and sonic transit time of brine which is 189 µs/ft.

Limitations of using this method:

1. The formula requires a physical model of the porous medium, representing it as a series arrangement of matrix and pore elements. While this approach simplifies calculations, it is an oversimplified representation that deviates significantly from the complexity of real rock formations.

2. A satisfactory fit between time-average-derived porosities and experimentally determined values is often difficult to achieve. This discrepancy can sometimes be resolved by incorporating variable matrix transit times for single-mineral lithologies or, in other cases, applying empirical correction factors to account for assumed under compaction effects. Raymer et al. (1980) extensively demonstrated these poor-fitting results.

Neutron and density Porosity

The integration of density and neutron logs offers a reliable source of porosity data, particularly in formations with complex lithology. This combination provides more accurate porosity estimates than using either tool or sonic logs alone, as it allows for better insights into lithology and fluid content. The values for density log were obtained from the seismic data in Kingdom software and converted to density porosity. Neutron porosity was obtained from seismic data as well. Both porosities were compared with the porosity in the lab, porosity derived from Wyllie time average equation and the porosity from the porosimeter.

3.5 Mavko-Jizba Equation

Mavko and Jizba (1991) presented simplified theoretical formulas to predict saturated rock moduli at very high frequencies, using dry rock pressure dependence as a basis. It corrects Gassmann's equation by considering the influence of pore shape and fluid mobility. The extended Mavko–Jizba squirt relations allow for the determination of saturated rock velocities and attenuation over a full spectrum of frequencies. To function, the model requires input data such as dry-rock elastic properties, dry-rock bulk modulus (at high pressure), solid and fluid bulk moduli, rock density, and porosity, all experimentally determined. Parameter Z, related to squirt-flow length, sets the frequency dispersion scale. Z is found by aligning theoretical and measured velocities at a chosen frequency. This calibration allows the model to predict velocities and attenuation for any frequency and pore fluid. The following are the assumptions of the extension of the Mavko-Jizba squirt equation:

1. the rock is isotropic;
2. all minerals making up the rock have the same bulk and shear moduli; and
3. fluid-bearing rock is completely saturated

Results of our experiment (density, porosity, bulk and shear moduli) were compared with the Mavko-Jizzba Equation.

Chapter 4 - Results

The results below cover the data obtained based on the laboratory ultrasonic, wireline logs of sonic and dipole-shear sonic, and porosity measurements. The rock core-plugs samples used in the pore-fluid fluid replacement and porosity measurements represent different depths in the Mississippian interval of Well Wellington KGS 1-32. The ultrasonic experiment was conducted for a range of ultrasonic frequencies. 20, 10, 5, 2.5, 1.25 MHz and, 156.3, 312.5, 625 kHz.

4.1 Dry Rock

The experiment started with 12 samples. The hydraulic jack was used to exert compressive stress initially to demonstrate overburden pressure. However, the samples were friable and could not withstand pressure so 3 samples were broken, leading to 9 samples being used for the dry rock experiment without the factor of pressure.

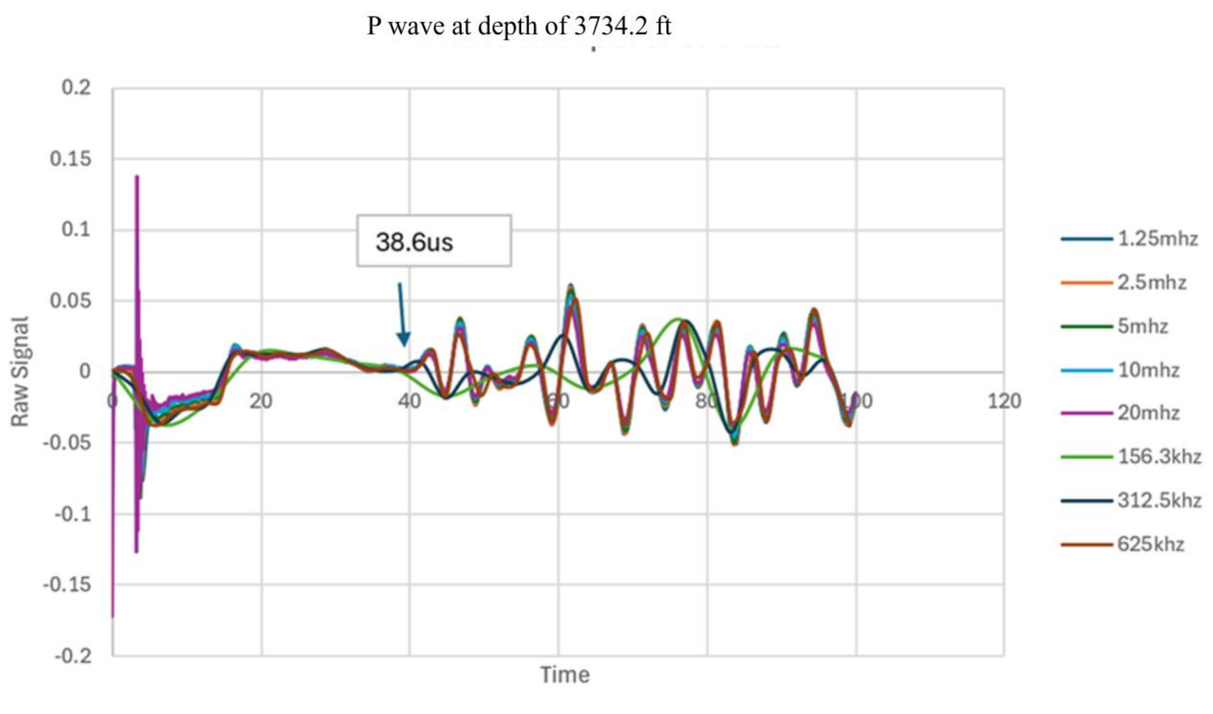

Figure 4.1 Graph showing P waves and first arrival time of the wave as well as different frequencies.

Fig. 4.1 has the P wave graph of a dry sample showing raw wave signal (y axis) plotted against time (x axis) for sample at depth of 3734.2 ft having first arrival time of 38.6micro-second with frequency varying between 625 kHz and 20 MHz superimposed on each other. Higher frequencies show a faster and closely packed waveform compared to lower frequencies. Higher amplitudes are also observed for the highest frequency and lower amplitudes for lowest frequency. First arrival time of P wave in Fig. 4.1, 38.6 micro-second is faster than first arrival time of S wave shown in Fig. 4.2 (41.6 micro-second) and that is expected since Primary waves are the first to arrive while S waves are slower and arrive much later. Also because of their slower speed, S waves appear to be more extended than the P wave.

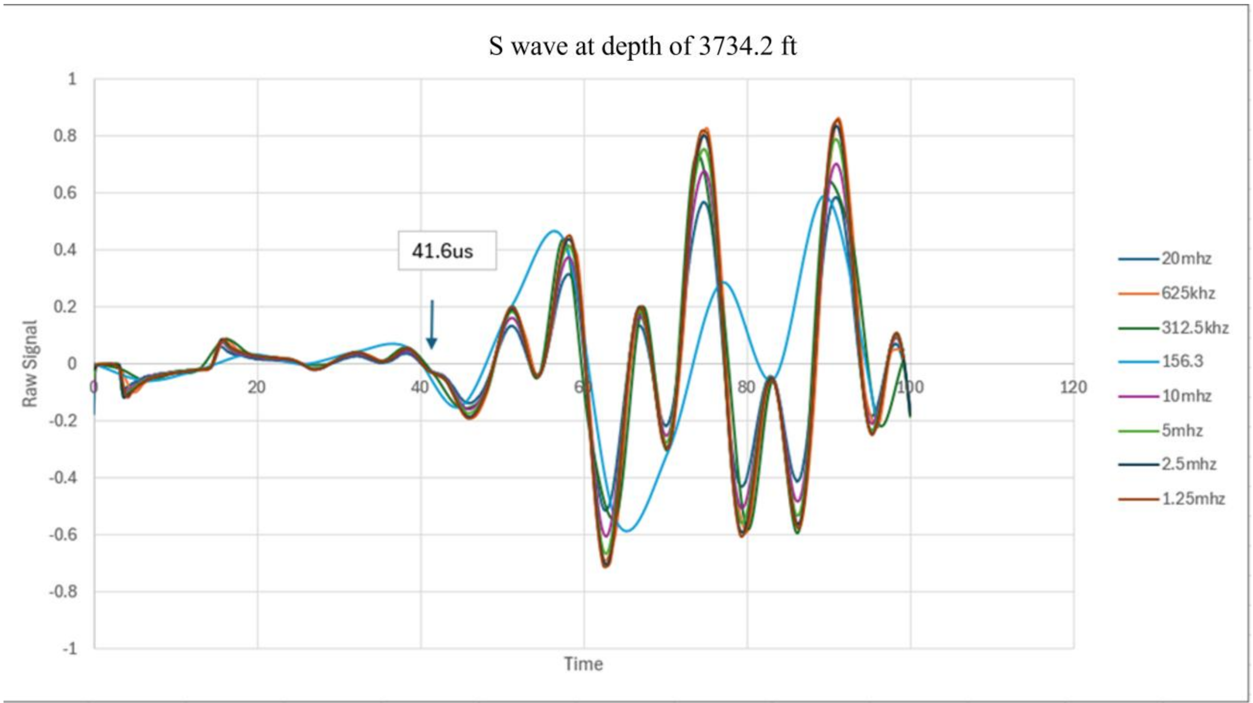

Figure 4.2 Graph showing S waves at the measured frequency and first arrival time (arrow).

4.2 Brine saturated rock

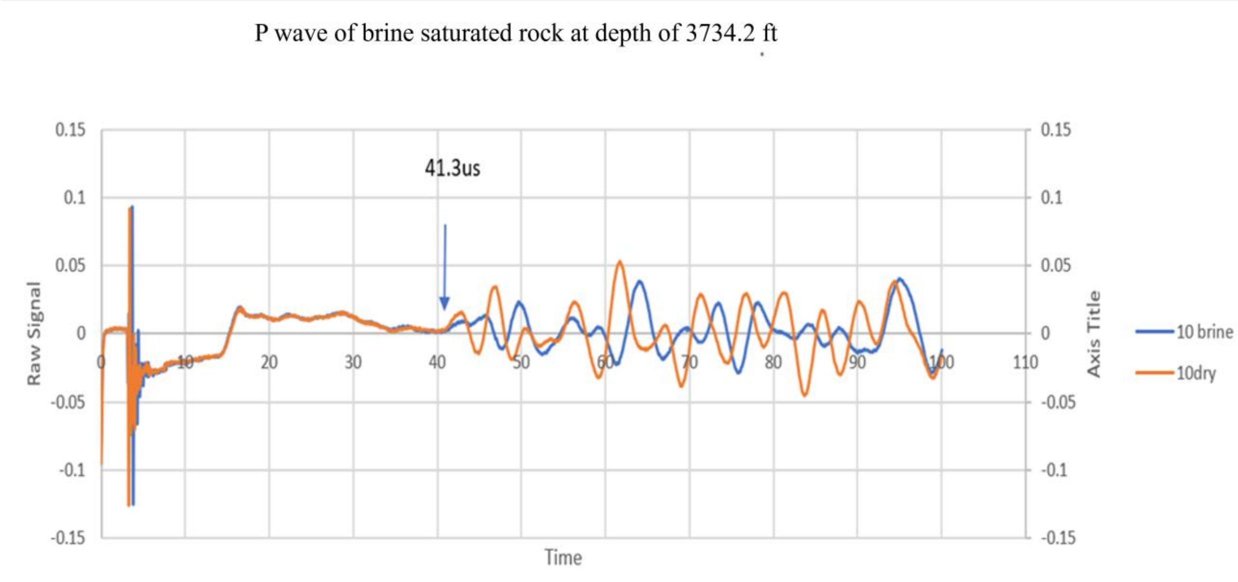

Figure 4.3 Graph showing P waves of dry sample superimposed with P wave of brine saturated sample at frequency of 10MHz and first arrival time.

The graphs in both Fig. 4.3 and Fig. 4.4 represent a P wave and S wave respectively and compare a dry and brine saturated sample at same depth of 3734.2 ft and at a frequency of 10MHz. The blue line is the brine saturated while the orange is the dry sample. The waveform of the brine saturated sample is seen to have a slower time of propagation ie velocity compared to the dry. Brine saturation causes a phase shift and slight attenuation which is evident in the amplitude difference between the dry and brine saturated samples. The amplitude difference in the S wave are more significant than the P. This is expected since S waves are more sensitive to fluid presence and fluid filles pores significantly impact shear wave propagation. Here as well, the P wave (Fig. 4.3) arrives much earlier -41.3 micro-second than the S wave (Fig. 4.4) which arrives at 42.5 micro-second. The P waves are seen to be more compressed than the S.

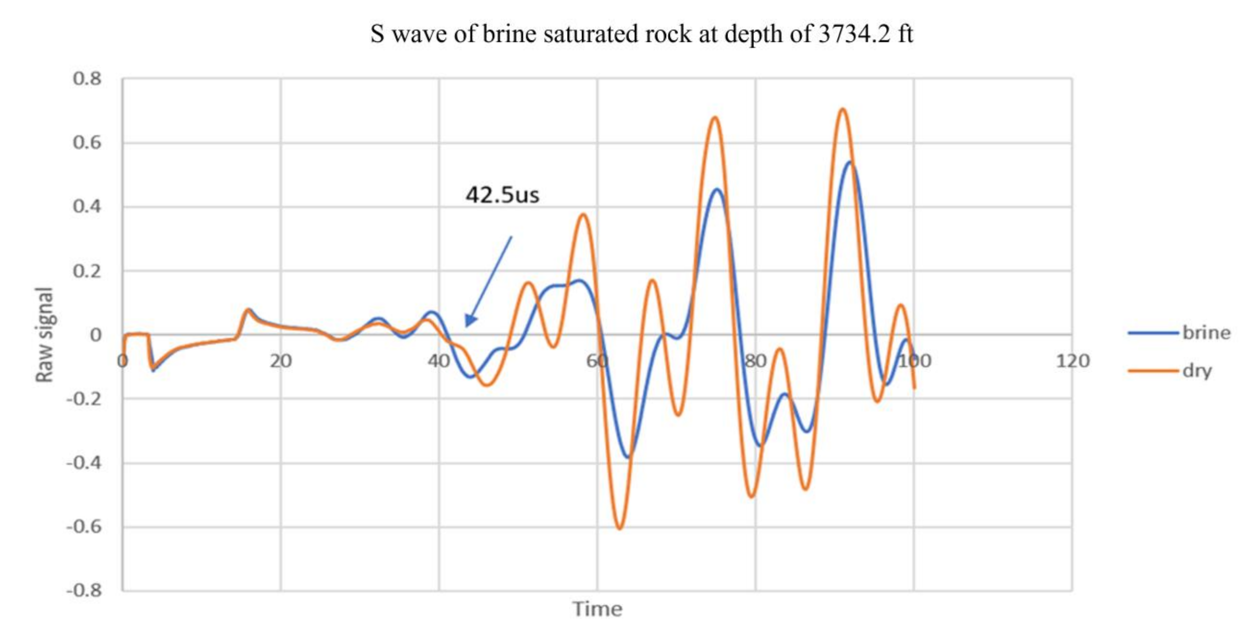

Figure 4.4 Graph showing Swaves of dry sample superimposed with Swave of brine saturated sample at frequency of 10MHz and first arrival time.

4.3 Partial Saturation of Brine

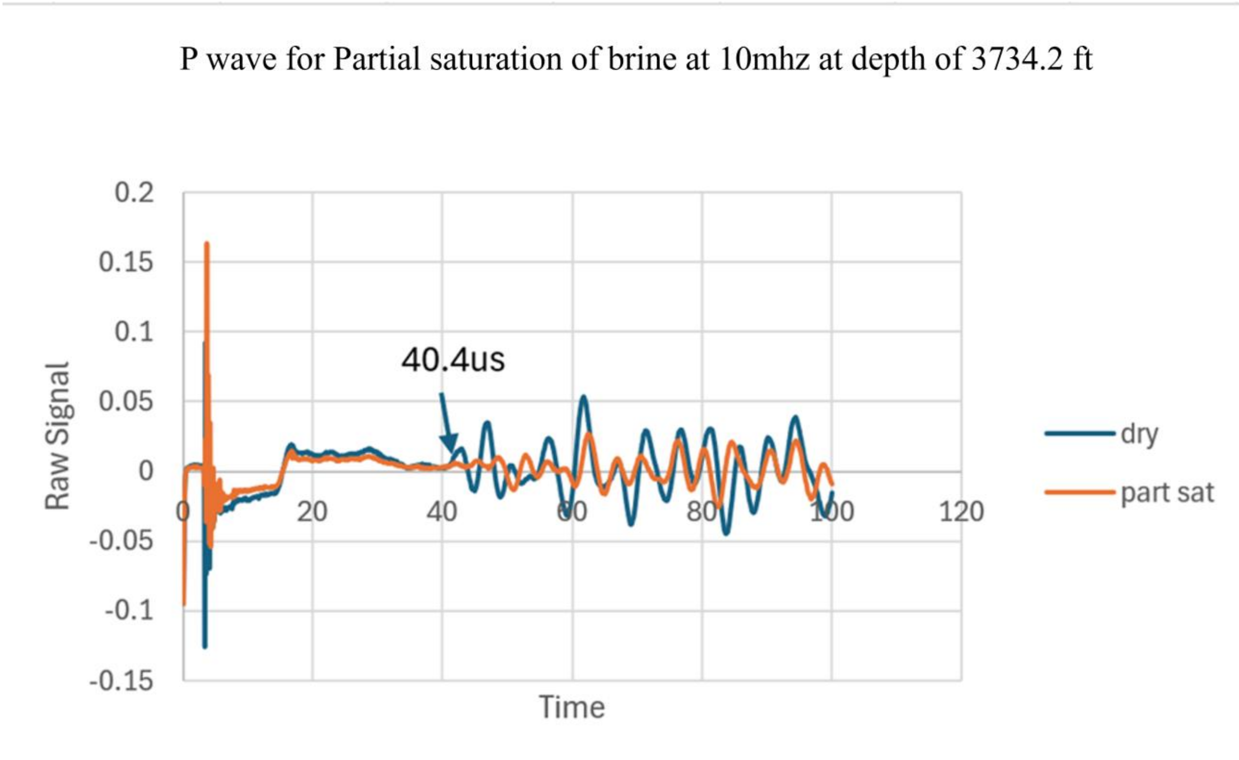

Figure 4.5 Graph showing P wave of partially saturated brine sample superimposed with P wave of dry sample and first arrival time; attenuation of the ultrasonic energy, in the case of partial saturation, is manifested as a reduction in amplitudes; velocity difference is obvious in this case by the delayed waveform of the partial saturation of the sample.

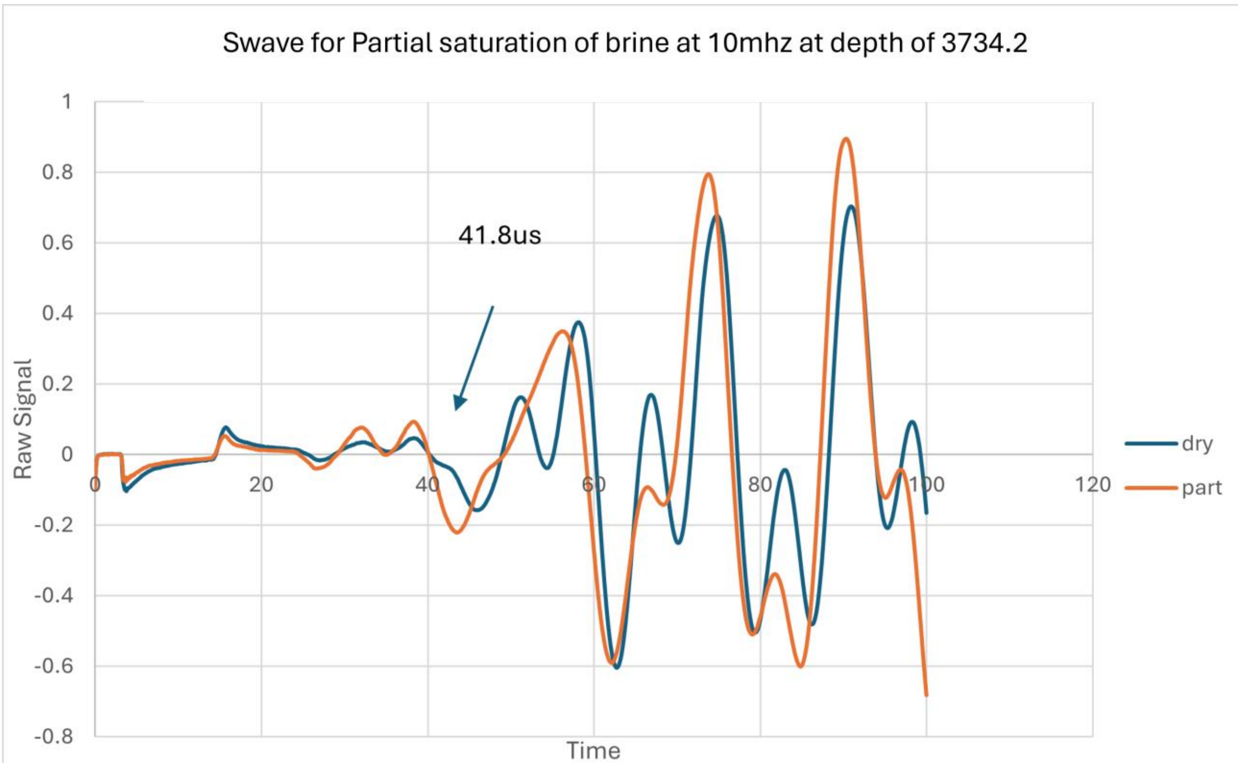

Figure 4.6 Graph showing Swaves of dry sample superimposed with Swave of partially saturated brine sample and first arrival time.

The respective first arrival time of the partially saturated rock in both P waves and S waves is delayed compared to the corresponding dry sample first arrival time. This suggests a slight decrease in velocity but not as pronounced as in the brine saturated sample. As seen in previous graphs, the S wave arrives at a later time than the P wave, as expected. The amplitude of the Swave of the complete brine saturation is much lower than the amplitude for the partial saturation of brine and dry sample. The attenuation effect in the partial saturation is moderate compared to the fully saturated brine sample. It is observed that full saturation has a greater impact on S waves than P waves; this is not seen in partial saturation.

4.4 Sum-total of saturations

Out of the 9 samples being used for the fluid substitution experiments, 4 of them had some parts of the rock chipping off when taking their velocity measurements. This affected their weight and subsequently the experiment hence only 5 of them were used to complete all saturations we needed to do (dry, brine, partially saturated brine, oil and brine saturation).

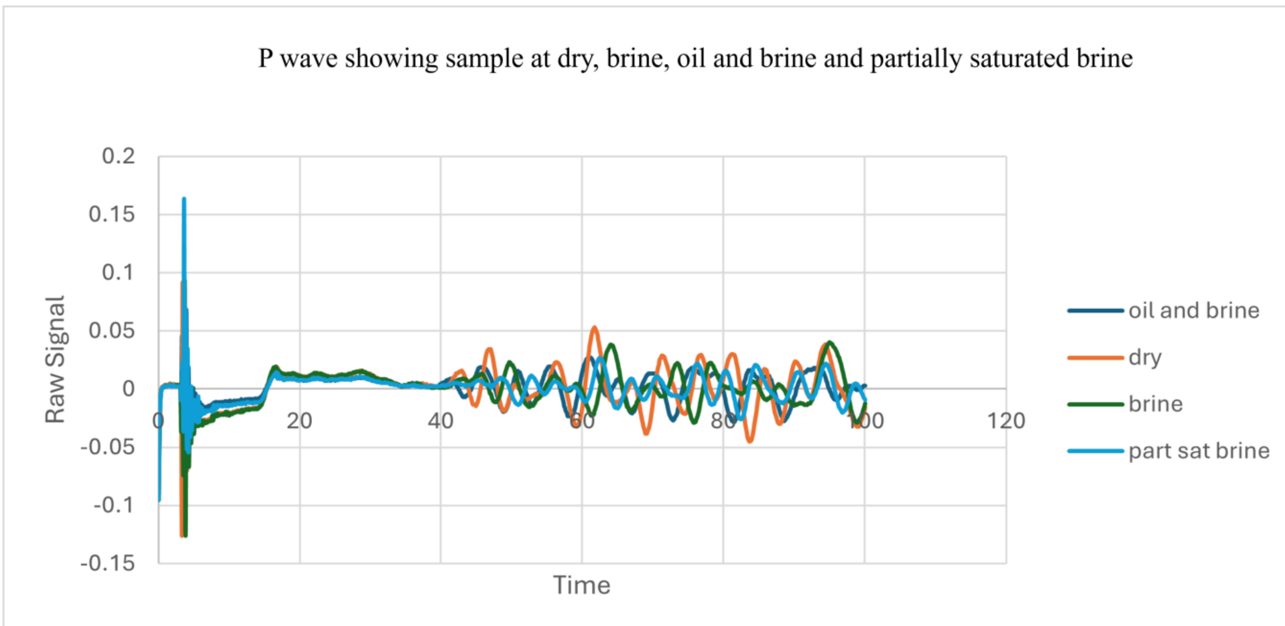

Figure 4.7 Graph showing P waves superimposed for dry, oil, brine and partially saturated brine sample at same frequency. Appendix A has the remaining samples used and the first arrival time for each.

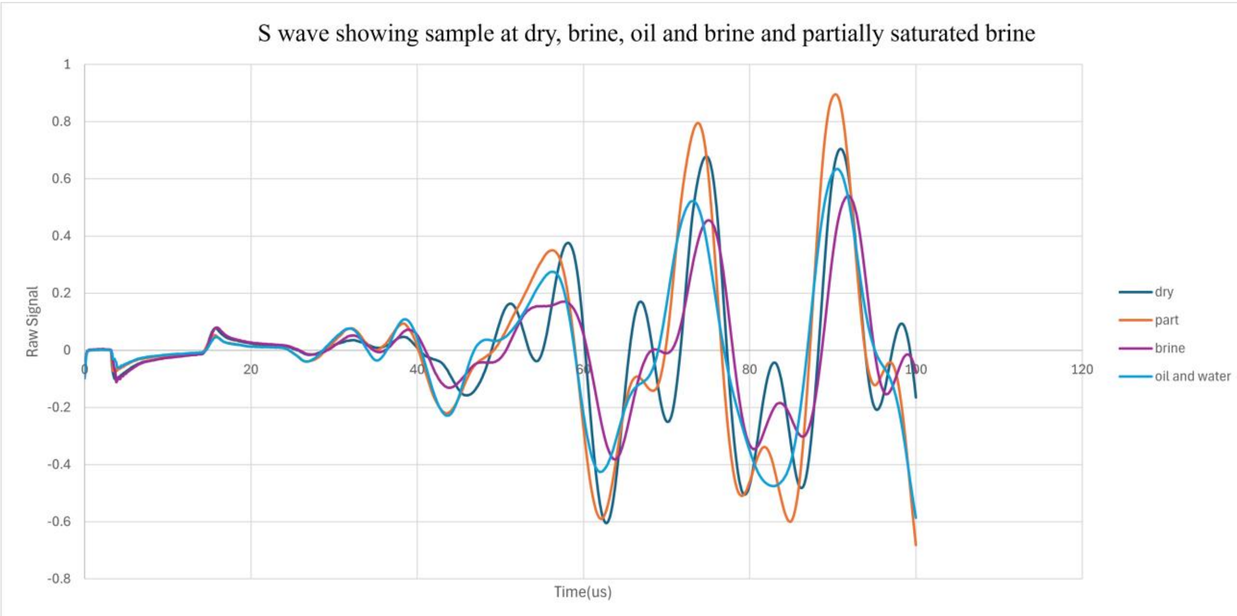

Figure 4.8 Graph showing Swaves superimposed for dry, oil, brine and partially saturated brine sample at same frequency. Difference in amplitude is as a result of the different fluid composition.

The graphs illustrate the P-wave signals and S-wave signals for rock sample at depth of 3734.2 at 10MHz under different saturation conditions: dry, brine-saturated, oil and brine-saturated, and partially brine-saturated. The x-axis represents time, while the y-axis shows the raw signal amplitude. Dry samples exhibit the highest peak amplitudes. Notably, significant amplitude variations associated with phase shifts are observed. In previous graphs, velocity changes for different fluid saturations were minimal, ranging from approximately 0.9–1.8 micro-second for P-waves and 0.2–0.9 micro-second for S-waves. The observed phase shifts and amplitude variations are attributed to dispersion effects.

Overall, attenuation provides a more effective means of identifying the type of pore fluid in a rock compared to velocity analysis.

4.5 Porosity Data

Depth	Velocity	Lab porosity	Porosimeter porosity	Density	Neutron	Wyllie's eqn
3936.6	4910.7	2.07	3.64	2.59	7.8228	10.0198
4096.2	5411.7	2.53	2.06	2.68	4.0362	6.166832
4076.5	5047.24	0.57	0	2.59	5.6371	9.042786
3734.2	5427.1	0.67	1.34	2.67	3.07	6.053678
3718.7	5025.5	6.66667	4.16	2.64	7.92	9.227935

Table 4.1 A table showing different porosity methods and associated values with the 5 samples.

The table (Table 4.1) gives the different sample depths with corresponding velocity values from sonic log and the different methods by which porosity was measured

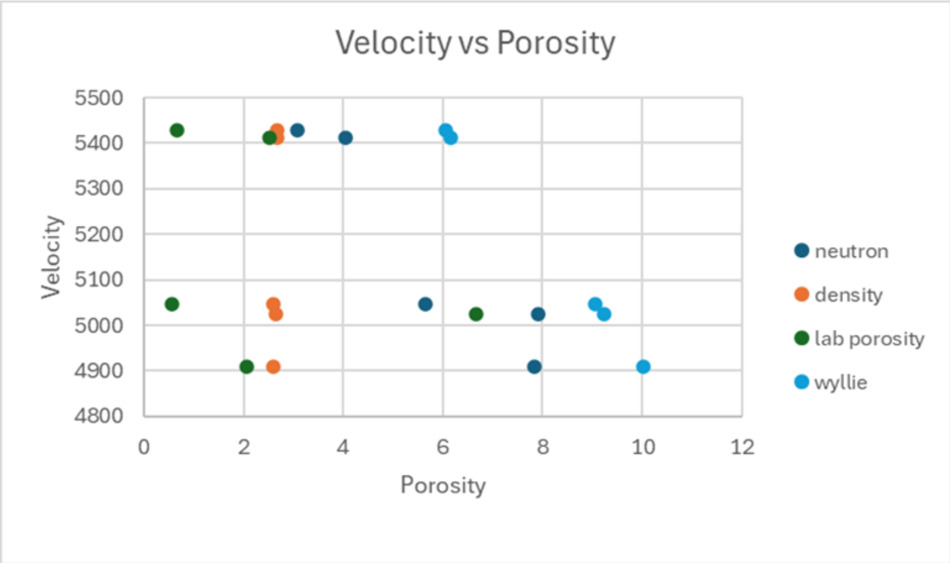

Figure 4.9 Velocity range of the 5 samples plotted against the different porosity methods; differences reflect complexity and limitations due to variation in the scale. Wyllie porosity (see text) seems to overestimate compared to the in-situ (well-log) porosities.

The graph in Fig. 4.9 plots the different velocities of each sample on the y axis and the different methods that was used to measure porosity on the x axis. The methods used to measure porosity were the fluid displacement method (lab porosity), the use of a porosimeter, neutron and density logs, and Wyllie's time average equation using the sonic log. Velocity calculated from the sonic log generally ranges from 4800-5500 m/s. Porosity values of these rock samples range between 0 and 11%. Velocity generally is decreasing as porosity increases, which is consistent with the expected trend that higher porosity results in lower velocity due to increased fluid content. The Wyllie equation data points appear to be more consistent, with a decreasing trend with increasing porosity compared to other methods. It is seen that using the Wyllie also gives a much higher porosity value compared to the different methods, at the same velocity.

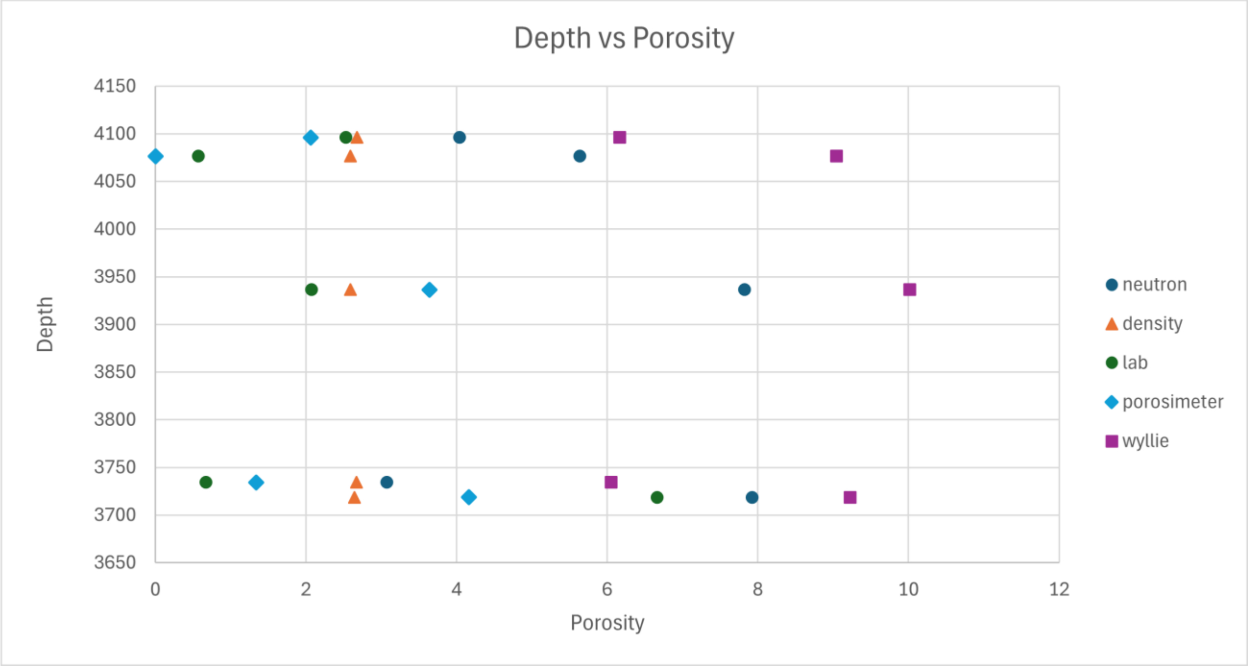

Figure 4.10 A plot of the different samples against different porosity methods.

The figure above (Fig. 4.10) illustrates the variation in porosity with depth, comparing multiple porosity estimation methods. The x axis represents porosity values, while the y- axis represents depth. The data shows significant variability in porosity values between different measurement methods. Neutron porosity exhibits consistently higher values at shallower depths while density porosity displays a broader range with some high porosity at greater depths. Laboratory and porosimeter porosity generally show lower porosity values. Wyllie's equation-based porosity follows a pattern that aligns with both log-derived and core-derived porosities but show some scatter due to its empirical nature. Porosity though, is generally decreasing with depth due to the effect of compaction and diagenetic processes.

4.6 Elastic Moduli-Poisson's Ratio

Sample	Frequency	Sonic Vp	Ultrasonic Vp	Sonic Vs	Ultrasonic Vs		Vp^2(ultraso	Vs^2	Poisson's Ratio(Ultrasonic)
3718.7	10 mhz	5025.5	4565.2	2942.5	2210.5		20841051	4886310.25	0.346869645
	5mhz		4565.2		2218.3		20841051	4920854.89	0.345452442
	20mhz		4500		2202.8		20250000	4852327.84	0.342433071
	2.5mhz		4500		2187.5		20250000	4785156.25	0.345289214
	1.25mhz		4632.4		2218.3		21459129.8	4920854.89	0.351228289
	156khz		5625		2045.5		31640625	4184070.25	0.423805621
	312.5khz		5625		2282.6		31640625	5210262.76	0.40143414
	625khz		4375		2157.5		19140625	4654806.25	0.339332304
									0.361980591
Sample	Frequency	Sonic Vp	Ultrasonic Vp	Sonic Vs	Ultrasonic Vs		Vp^2	Vs^2	Poisson's Ratio
3734.2	10 mhz	5427.1	5833.3	3158.1	2611.9		34027388.9	6822021.61	0.374619932
	5mhz		5303.3		2447.6		28124990.9	5990745.76	0.364672463
	20mhz		5054.2		2486.7		25544937.6	6183676.89	0.340308
	2.5mhz		4605.3		2430.6		21208788.1	5907816.36	0.306946367
	1.25mhz		7291.7		2464.8		53168888.9	6075239.04	0.43549832
	156khz		6250		2272.7		39062500	5165165.29	0.423811631
	312.5khz		6250		2272.7		39062500	5165165.29	0.423811631
	625khz		6250		2536.2		39062500	6432310.44	0.401436208
									0.383888069

Table 4.2 P and S wave ultrasonic and sonic velocities.

The table above(Table 4.2) shows the different samples with the different ultrasonic frequencies measured in the lab, the corresponding velocity of that depth from the sonic log.

From the Velocity, Poisson’s ratio was calculated to determine the elastic moduli of the rocks. This was done for all 5 samples and the average was calculated for each of them.

Depth(ft)	Poisson's Ratio
3718.7	0.36
3734.2	0.38
4076.5	0.39
4096.2	0.39
3936.6	0.29

Table 4.3 Poisson’s ratio values for respective depths.

The table (Table 4.3) above shows each depth measured in feet with corresponding Poisson’s ratio. Poisson’s ratio fell in the range of 0.29- 0.39, indicating variation in rock geomechanical properties at different depths; lower Poisson’s ratio indicates higher brittleness.

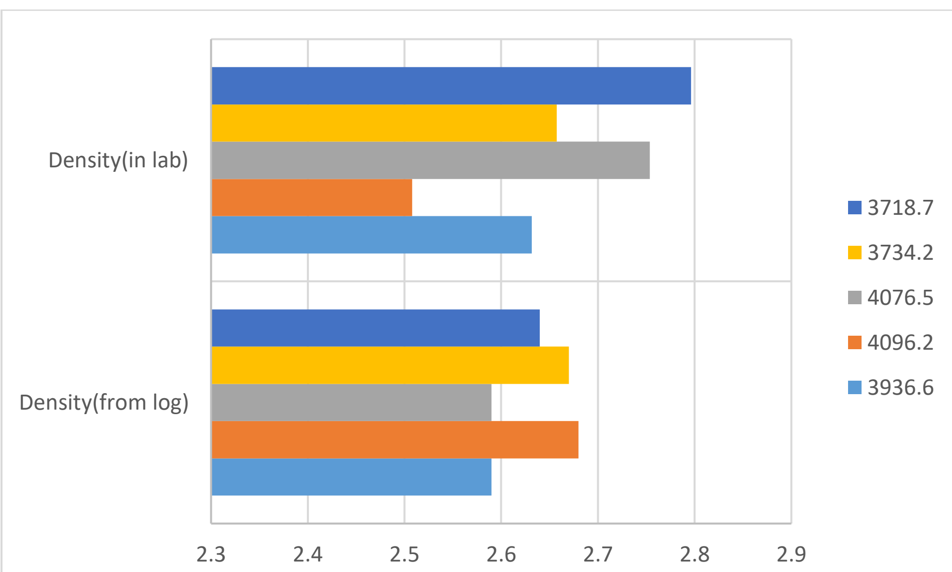

Figure 4.11 Density from lab calculations vs density values from logs.

Chapter 5 - Discussion

Based on the experimental ultrasonic Vp and Vs waveforms, variation in amplitude and attenuation are strongly attributed to pore fluid types. In Fig. 4.7 we see different amplitudes of waveforms that exhibit different states of the rock including when it was dry and when it was filled with brine as well as when it was filled with a mix of oil and brine. The dry rock showed the highest amplitude followed by the brine and finally partially saturated brine and oil. This is caused by the attenuation effect. A higher attenuation results in a greater amplitude reduction due to the fluid presence. From here, it is observed that a rock with brine may show a higher amplitude than a rock that has hydrocarbon present in it. Analyzing seismic data amplitude has proven valuable for determining variations in key petrophysical parameters, including lithology, porosity and fluid saturation (Varela et al., 2006). Attenuation occurring in both P and S waves are very helpful and can be useful in locating dry reservoirs.

As seen below in Figs. 5.1 and 5.2, both P and S wave attenuation related attributes can be helpful in identifying producing hydrocarbon formations. Dry samples will always show high amplitudes. This corroborates a study of the Viola formation in Clark County. According to Vohs (2016), seismic amplitude analysis revealed that the top of the productive Viola carbonate facies was characterized by lower amplitudes. Producing wells were associated with these lower amplitudes, while dry holes and uneconomical wells showed higher amplitudes.

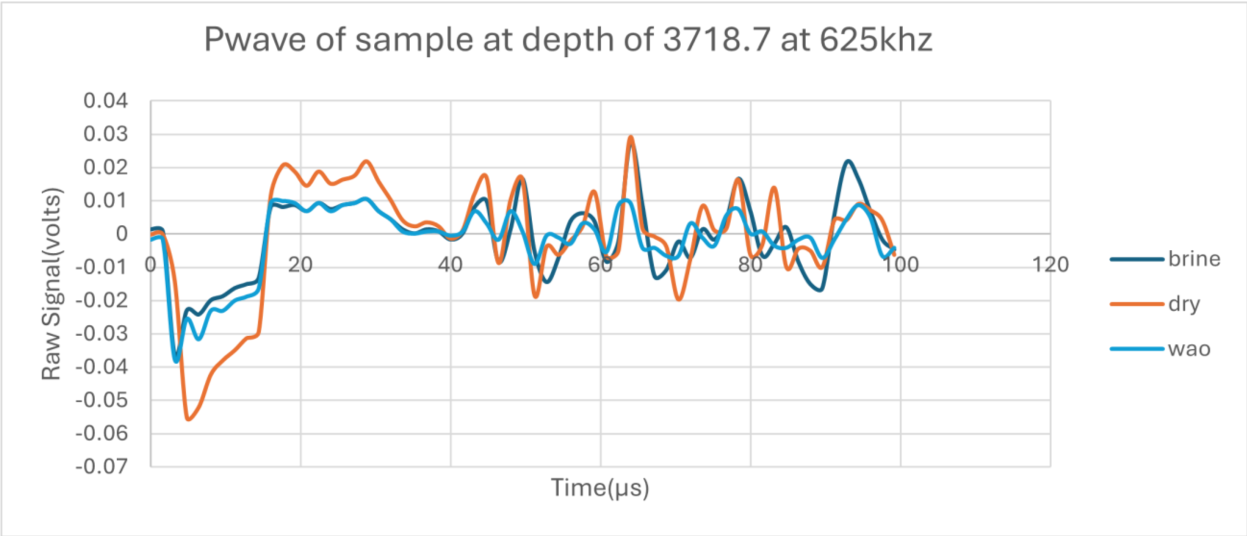

Figure 5.1 P wave energy attenuation at sample 3718.7 which was extracted from 3718.7 ft depth; the presence of hydrocarbon causes higher attenuation, thus reduction in amplitude (energy).

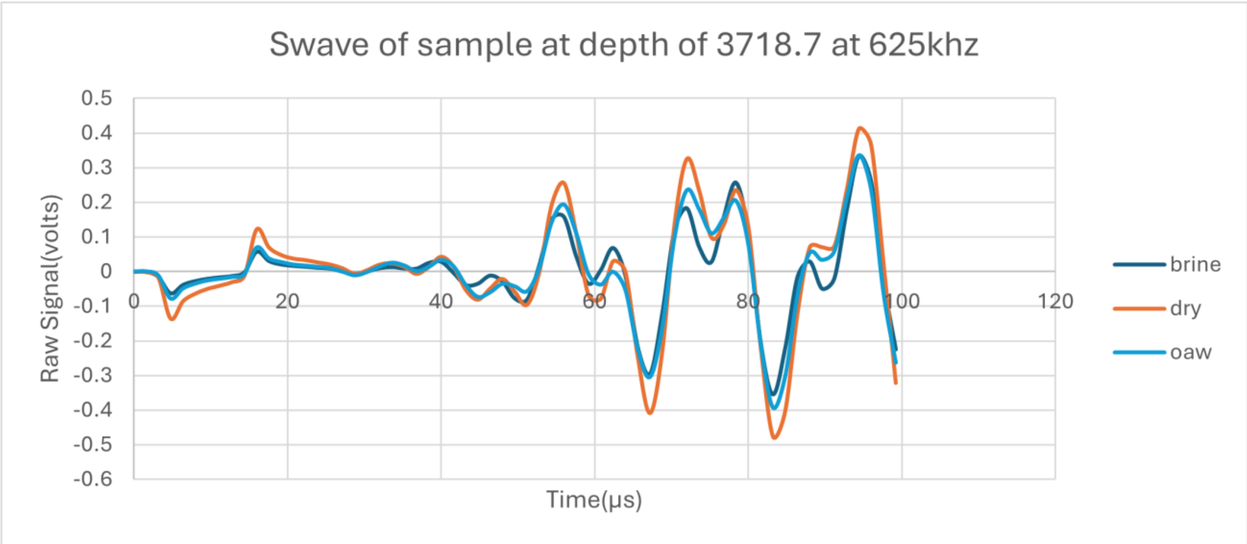

Figure 5.2 S-waveform and observed attenuation effects on amplitude for sample at depth of 3718.7.

Our ultrasonic velocity results were compared to the Mavko-Jizba model using python and resulted in the Fig. 5.3 and Fig. 5.4 plots below:

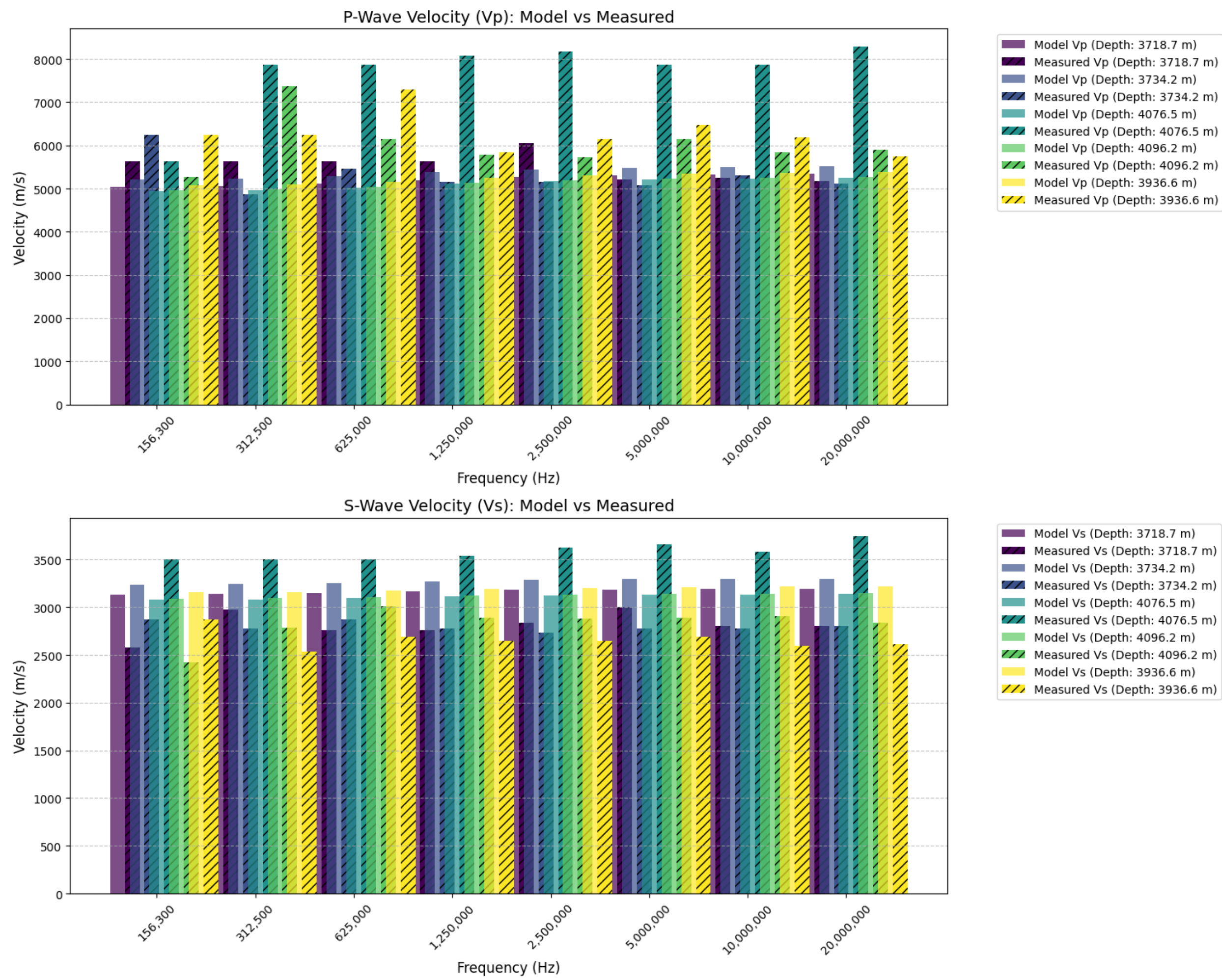

Figure 5.3 A graph of measured P and S velocities plotted with the Mavko-Jizba model predicted velocities.

The graph compares the measured velocities in the lab to the velocities developed by the model (Mavko-Jizba). As frequency increased, the velocity of each sample increased as well. Velocity also increased with increasing depth, agreeing to the effect of compaction and low porosity. The measured velocity value at each frequency is higher than the model prediction (except at very high frequencies at 5mhz when 3734.2 and 3718.7 both have the models being greater than measured). For Swaves, all the models are higher than the measured, except 4076.5 Hence, in this case, the model was not able to predict the behavior of the rock, the discrepancy is significant for one sample. This could be due to its limitation of assuming complete saturation. Our measured and modeled Vp and Vs were plotted on a scatter plot and resulted in this graph.

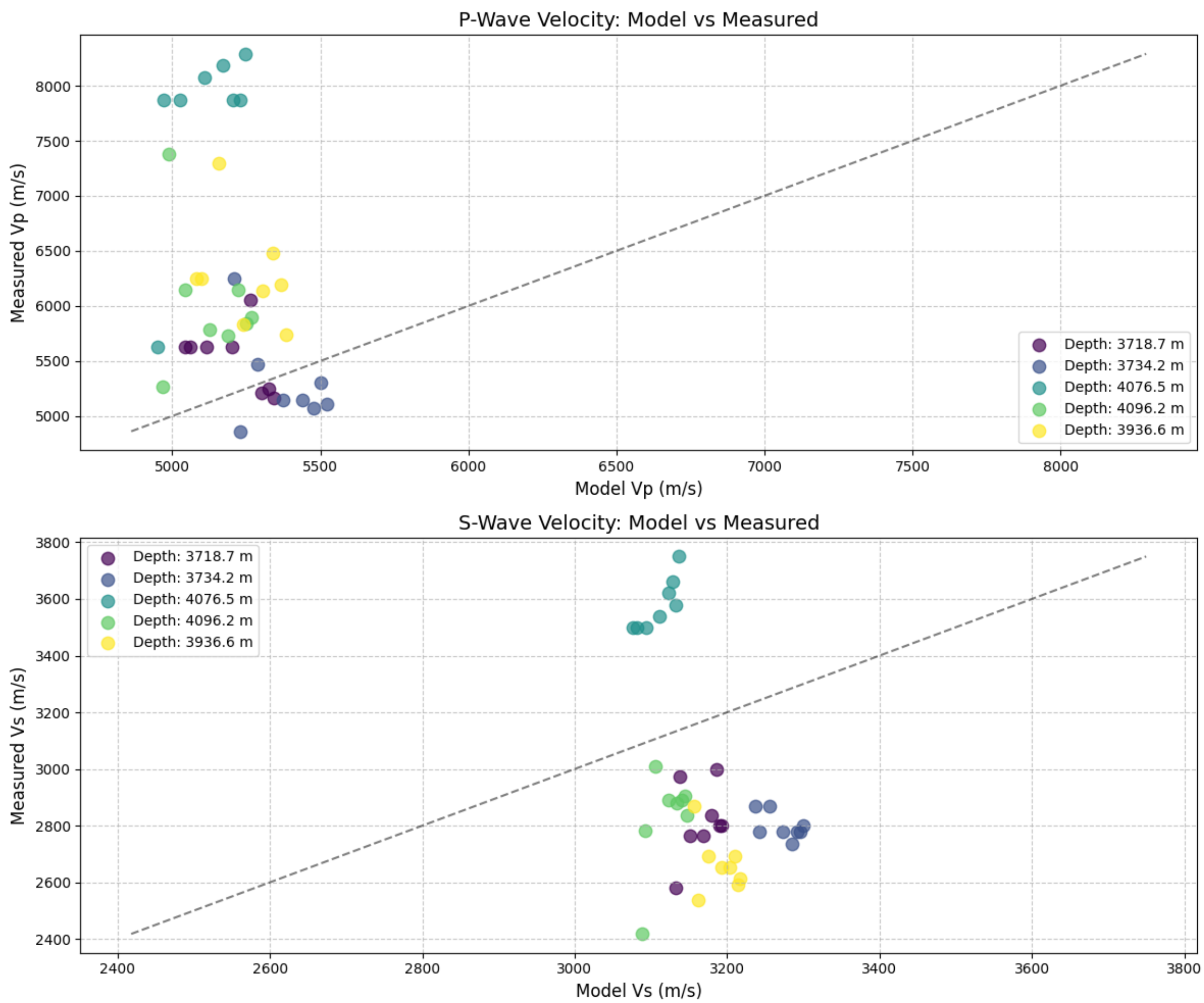

Figure 5.4 A graph showing a measure of the correlation between measured velocities and Mavko Jizba model velocities; the model overestimated for all the samples but one.

From the above we see Measured Vp and Vs on the y axis and modeled Vp and Vs on the x axis. The dashed line represents the 1:1 line meaning perfect agreement between the model and measured values. Measured Vp is higher than model Vp (above the dashed line). At velocity of 6000 m/s the difference becomes even more pronounced. This means that the model underestimates Vp . This could be as a result of pore fluid effects (fluids will stiffen the rock frame in a way that is not fully captured by the model), mineralogical variations and fluid dispersion.

Measured Vs is however lower than modeled Vs values which means Vs was overestimated by the model. This could also be because of fluid presence (fluids weaken shear wave propagation which reduces Vs more than expected) and Squirt flow effects which are more pronounced in Vs due to shear wave interaction with pore spaces.

The following set of cross plots in Fig. 5.5 & Fig. 5.6 compare the ultrasonic Vp and Vs with well-log scale in situ Vp and Vs and overlays published models of dolomite Vp-Vs. and Vp versus Vp/Vs.

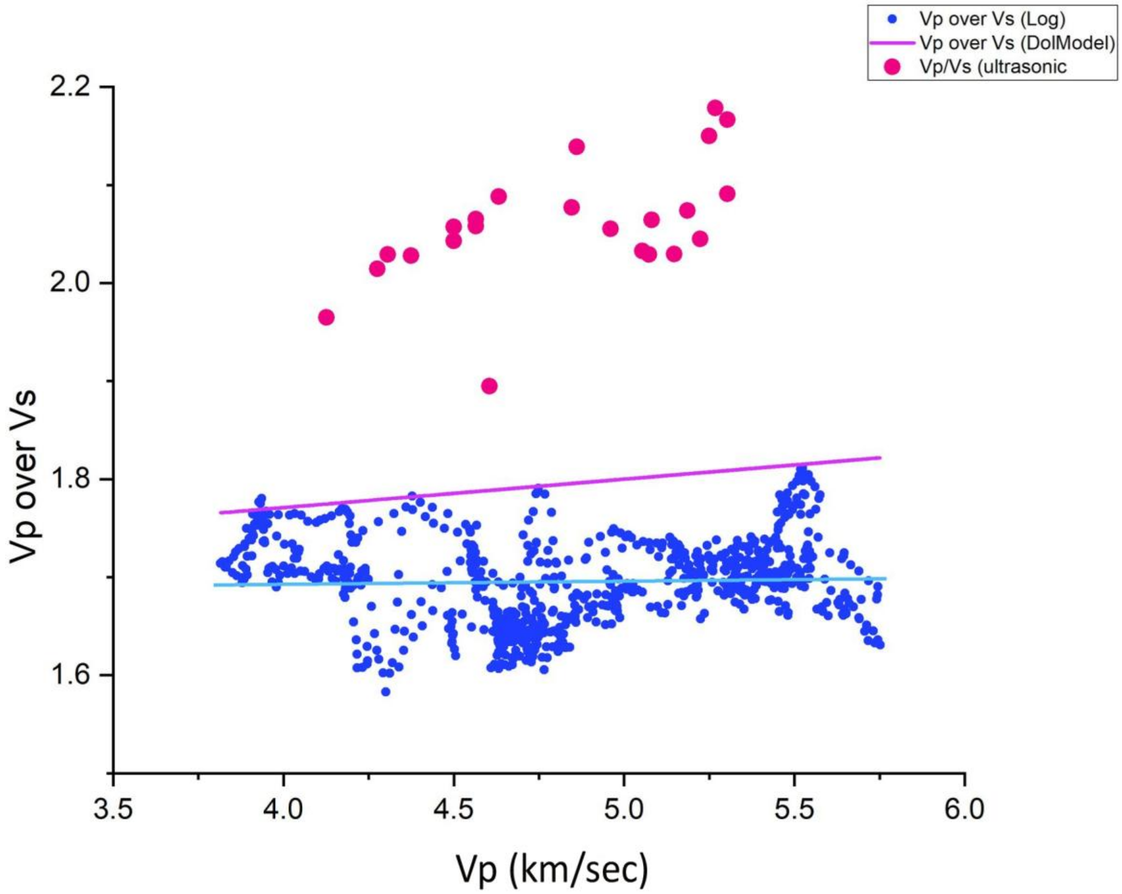

Figure 5.5 Vp/Vs plotted against P velocity for ultrasonic dry sample and log data.

Blue points are the Vp/Vs ratio from well logs of KGS 1-32 and the blue line is its best linear fit. The pink dots are the Vp/Vs from ultrasonic measurements and the pink line is best fit trend for modeled Dolomite (Dolmodel) using the Yale and Jamieson (1994) model. It is seen here that the ultrasonic Vp/Vs values are higher than log-derived values. This is because ultrasonic measurements are at MHz frequencies while logs are in kHz leading to differences in dispersion. Also logs reflect in-situ conditions with possible fluid saturation, while ultrasonic measurements were made for dry samples and hence may not fully capture squirt flow and fluid effects in the same way. This leads to much higher Vp/Vs ratio for dry samples than brine saturated. Log data show a more stable trend with Vp with only slight increase in Vp/Vs as Vp increases. Ultrasonic data however shows a scattered and increasing trend, suggesting that at lower velocities, Vp/Vs is more variable and less predictable in lab conditions.

Ultrasonic Vp/Vs values are higher than the Yale and Jamieson model which is due to the absence of pore fluids in the ultrasonic measured dry samples. The contrast between dry ultrasonic and well log data highlights the significant role of fluid saturation in reducing Vp/Vs ratio. Also, the best-fit trend line for logs is below the Yale & Jamieson model which suggests gas saturation in some zones due to the lower Vp/Vs.

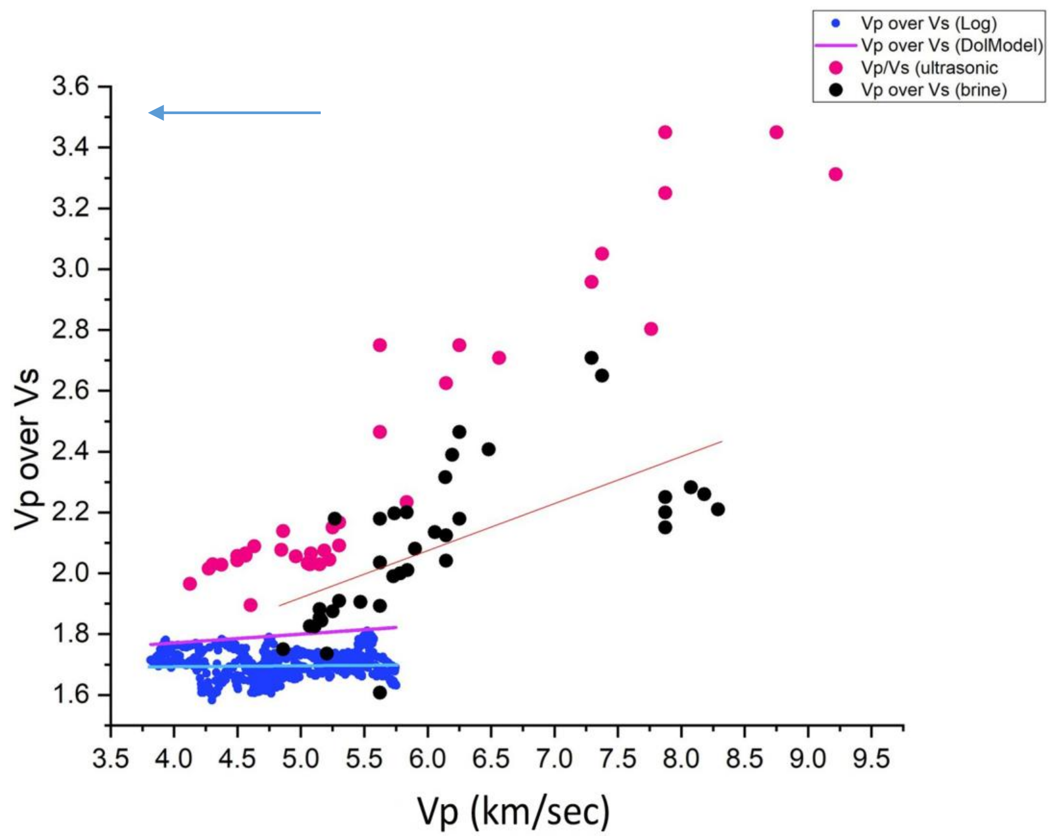

Figure 5.6 Vp/Vs plotted against P velocity for ultrasonic dry & brine samples and log data.

The blue dots are Vp/Vs ratio from well log data; the pink dots are Vp/Vs ratio from ultrasonic dry samples, the black Vp/Vs ratio from brine saturated ultrasonic samples. The blue line provides the best fit for well log data, the pink line is best fit trend for the Yale and Jamieson (1994) model, and the red is the trend of best fit for brine saturated ultrasonic samples. The arrow shows direction of increasing porosity.

The well log data shows a stable Vp/Vs trend across increasing P wave velocity. This trend suggests that Vp/Vs is well constrained for brine-saturated formations at seismic frequencies. The Vp/Vs increases as Vp increases in the dry samples. This is because of the overestimation of Vs. The Yale and Jamieson (1994) model is slightly above the well log trend, indicating their model predicts slightly higher Vp/Vs than real well log data.

Brine saturated ultrasonic data is between the dry samples and well log trends, This is because the fluid will have a lower Vp/Vs than in dry samples, (due to the reduction in Vs as a result of shear waves propagating through a fluid) however Vp/Vs is slightly higher than well log values due to frequency differences and difference in fluid distribution in the lab compared to a real reservoir.

Well log trend (blue line) lies lower than both Yale & Jamieson(1994) model and ultrasonic brine data. This suggests that field conditions lead to a slightly lower Vp/Vs ratio than what models predict. This could be due to compaction and cementation reducing Vp/Vs in actual reservoirs. Well logs remain the most reliable in-situ Vp/Vs values for reservoir characterization. Porosity is increasing towards lower velocities. Brine saturation lowers Vp/Vs. The brine saturated data seems to coincide with the well-log scale data for velocities less than 5.5 Km/sec. The implication of this relation points to the validity of utilizing Vp/Vs to convert in situ well-log Vp to Vs for wells that lacks dipole shear sonic logs.

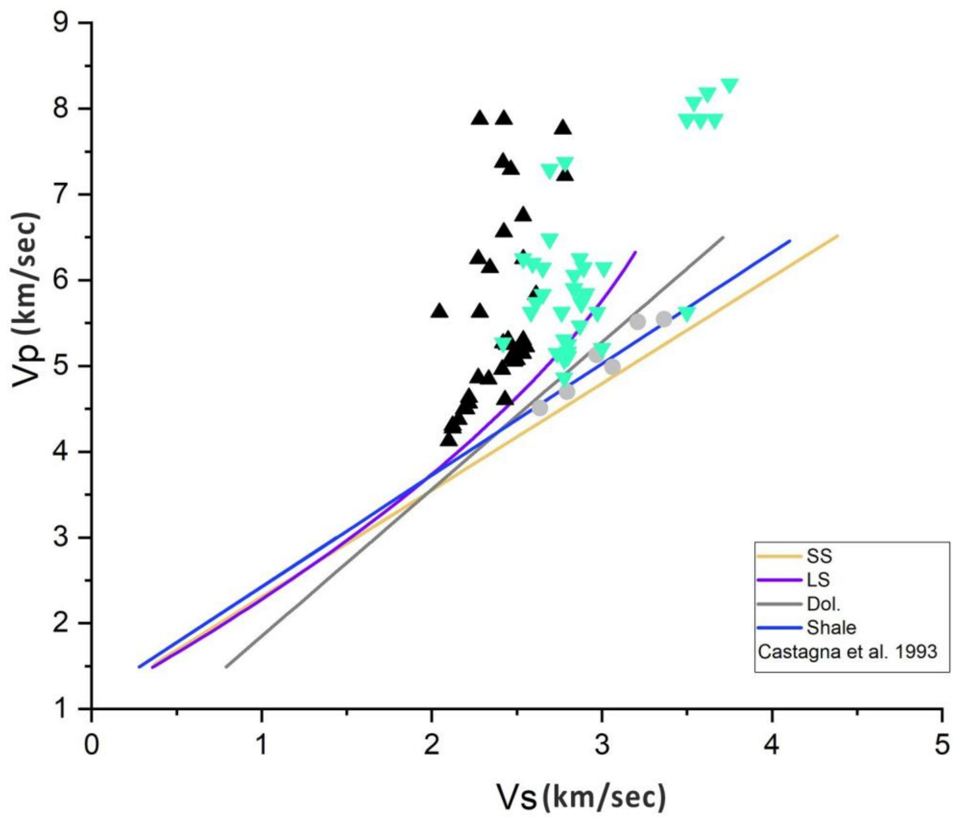

Figure 5.7 Dry, brine and well log data plotted on Castagna model to determine lithology.

The plots in Fig. 5.7 & Fig. 5.8 show the Vp vs Vs relationships for dry (black triangles), brine saturated (cyan triangles) and well log data (gray circles) compared to lithology models from Castagna et al (1993) for different rock types.

Castagna et al (1993) models provide a good baseline for lithology classification in seismic/ well log interpretations. Well log values follow expected in-situ behavior and align more closely to the lithology models, compared to brine saturated and dry samples which plot above the models. This confirms that log scale Vp-Vs are more reliable for reservoir interpretation. From the well data, the plots fall closer to dolomite confirming the lithology of interest.

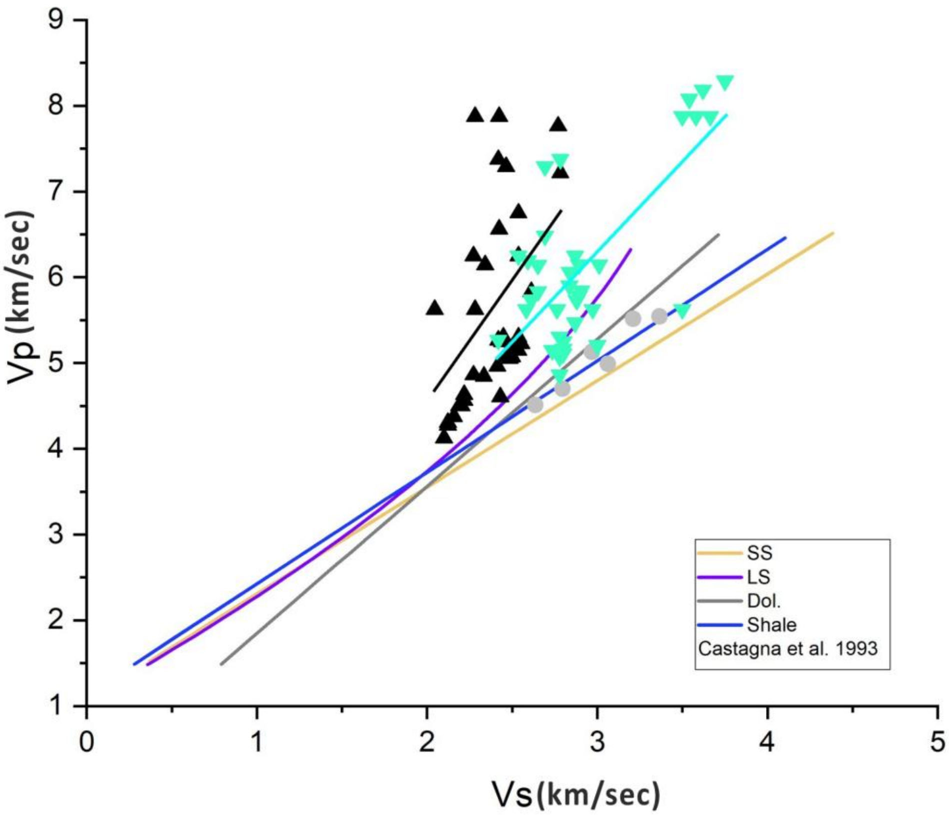

Figure 5.8 Dry, brine and well log data plotted on Castagna model along with lines of best fit for dry and brine.

The plot above shows the best-fit trend line for both dry and brine-saturated samples. The best-fit black trend line is steeper than the cyan line of best fit as well as the models. Contrary to the conventional expectation that fluid saturation lowers Vs, the brine saturated samples here exhibit higher Vs values than dry samples. This behavior could be due to the pore-fluid stiffening effect, which is particularly common in carbonates where brine fills pores and reduces pore-space compressibility. This effect is more pronounced at ultrasonic frequencies where squirt flow effects are suppressed. The brine saturated samples align a bit closer to the well log data which falls on the model. This confirms that fluid saturated lab measurements provide a better approximation of in-situ conditions than dry rock measurements because dry rocks do not account for fluid interactions that occur at reservoir conditions.

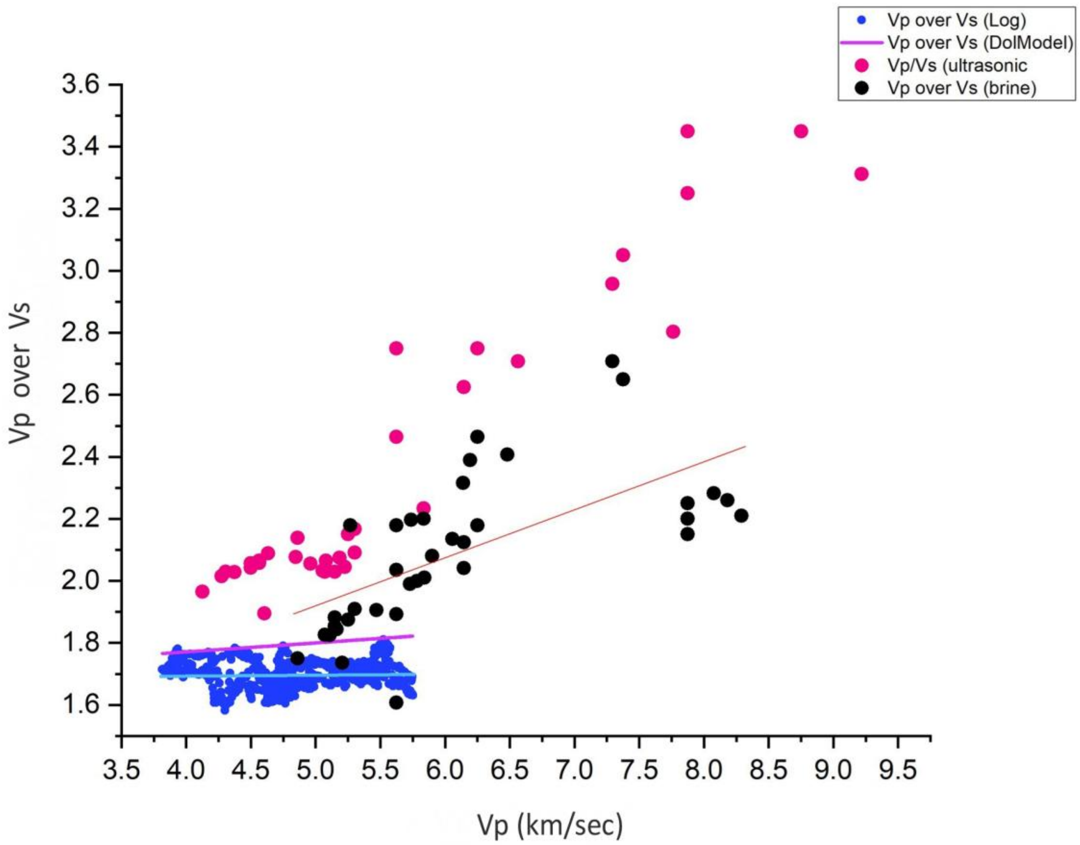

(a)

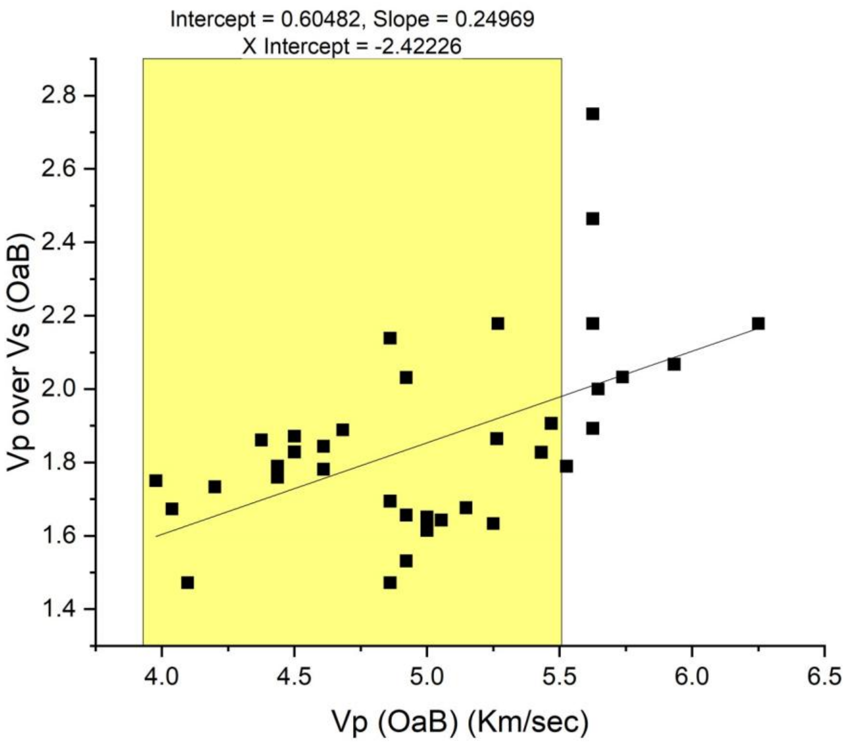

(b)

Figure 5.9 (a) Different fluid saturations (dry, brine and oil&brine) in the lab plotted with well log data , (b) Ultrasonic data for mixed saturation of brine and oil with best fit to identify intercept Vp/Vs for velocities less than 5.5 km/sec.

The Vp/Vs cross plot in Fig. 5.9a provides key insight into the impact of fluid saturation on seismic velocities. This dataset includes dry samples (pink), brine saturated samples (black), oil and brine samples(green), and well log data (blue) with trend lines highlighting the variations across different conditions.

The dry samples have the highest Vp/Vs ratios, particularly at higher Vp. In brine saturated samples, Vp/Vs values are lower than dry samples, however this is still slightly higher than well logs. However, in Oil and brine saturated samples (green dots), Vp/Vs values fall between brine-saturated and well log data suggesting that a mixture of oil and brine represents real reservoir conditions. The oil and Brine trend aligns more closely with well logs, reinforcing the idea that natural hydrocarbon reservoirs have a mix of both oil and brine rather than pure brine.

The brine saturated data seems to coincide with the well-log scale data for velocities less than 5.5 Km/sec, as indicated in (b) above. This relation implies the validity of utilizing Vp/Vs to convert in situ well-log Vp to Vs for wells that lack dipole shear sonic logs. Better reservoir properties, fortunately correlate with lower velocities, thus the utility of this relationship for the range of velocities observed for carbonate reservoirs.

Chapter 6 - Conclusion

This study demonstrated that attenuation is a highly effective indicator of pore fluid composition, making it a valuable tool for enhancing reservoir seismic characterization for carbonate lithologies. Identifying areas of high attenuation can help optimize hydrocarbon targeting while reducing the risk of drilling dry wells. When combined with other seismic attributes and geophysical log analysis, attenuation measurements can significantly improve monitoring of CO_2 sequestration and enhanced oil recovery (EOR) in carbonate formations. Although these formations exhibit relatively low porosity, their suitability for CO_2 injection largely depends on permeability and the presence of natural fractures in the subsurface. For brine-saturated samples, the ultrasonic Vp and Vs estimates seem to coincide with the well-log scale data for velocities less than 5.5 Km/sec, as indicated above. This relation implies the validity of utilizing Vp/Vs to convert in situ well-log Vp to Vs for wells that lack dipole shear sonic logs. Better reservoir properties, fortunately correlate with lower velocities, thus the utility of this relationship for the range of velocities observed for carbonate reservoirs. The discrepancies with the tested Mavko-Jizba model and other linear-fit Vs-Vp and Vp versus Vp/Vs warn against utilizing these models for the Mississippian carbonates. Future research should incorporate in-situ conditions, including reservoir pressure, to better simulate the subsurface. Additionally, using longer core plugs would provide deeper insights into velocity behavior under varying fluid saturations, while increasing the number of samples analyzed would enhance the statistical robustness of the findings. By providing new insights, this research advances reservoir characterization methodologies, thereby supporting improved hydrocarbon recovery and carbon sequestration within carbonate formations.

References

Adam, L., & Batzle, M. (2008). Elastic properties of carbonates from laboratory measurements at seismic and ultrasonic frequencies. *The Leading Edge, 27*(8), 1026–1032.

Adam, L., Batzle, M., & Brevik, I. (2006). Gassmann's fluid substitution and shear modulus variability in carbonates at laboratory seismic and ultrasonic frequencies. *GEOPHYSICS, 71*(6), F173–F183.

Adkison, W. L. (1972). Stratigraphy and structure of Middle and Upper Ordovician rocks in the Sedgwick Basin and adjacent areas, south-central Kansas (No. 702). *US Geological Survey*.

Akpan, A. S., Okeke, F. N., Obiora, D. N., & Ibuot, J. C. (2020). Fluid substitution modeling and derived rock attribute-based discriminations of hydrocarbon reservoirs in the Niger Delta. *Journal of Petroleum Exploration and Production Technology*.

Aminzadeh, F., & Dasgupta, S. N. (2013). Reservoir characterization. In *Developments in Petroleum Science* (Vol. 60, pp. 151-189). Elsevier.

Bakhorji, A. M. (2010). Elastic anisotropy and seismic reservoir characterization of carbonate rocks (Doctoral dissertation, University of Alberta).

Birch, F. (1961). The velocity of compressional waves in rocks to 10 kilobars. *J. Geophys. Res. 66,* 2199–2224. https://doi.org/10.1029/JZ065i004p01083.

Cahill, T. E. (2014). Subsurface sequence stratigraphy and reservoir characterization of the Mississippian limestone (Kinderhookian to Meramecian), south central Kansas and north central Oklahoma. University of Arkansas.

Carr, T. R., Green, D. W., & Willhite, G. P. (1998). *Improved oil recovery in Mississippian carbonate reservoirs of Kansas: Near-term—Class 2*. Annual report. Kansas Geological Survey.

Cimino, V. (2020). A rock physics modeling approach in analysis and integration of well logs and ultrasonic velocities for characterizing the reservoir facies of the Viola Limestone in southwestern Kansas.

Deng, W., & Morozov, I. B. (2017). Trade-off of elastic structure and Q in interpretations of seismic attenuation. *Pure and Applied Geophysics, 174*(10), 3853–3867. https://doi.org/10.1007/s00024-017-1581-3

Dolton, G. L., & Finn, T. M. (1989). *Petroleum geology of the Nemaha uplift, central midcontinent* (USGS Open-File Report 88-450D). U.S. Geological Survey.

Evans, C. S., & Newell, K. D. (2013). The Mississippian Limestone Play in Kansas: Oil and gas in a complex geologic setting. *Kansas Geological Survey, Geology Extension, University of Kansas*. http://www.kgs.ku.edu/Publications/PIC/pic33.html

Fadolalkarem, Y. (2015). Pre-stack seismic attribute analysis of the Mississippian Chert and the Arbuckle group at the Wellington field, south-central Kansas. Submitted to the graduate degree program in Geology and the Graduate Faculty of the University of Kansas.

Fritz, R. D., & Medlock, P. L. (1995). Recognition of unconformities and sequences in mid-continent carbonates.https://archives.datapages.com/data/tgs/tgs-sp/data/047/047001/49_tgs-sp0470049.htm

Franseen, E. K. (2006). *Origin of Upper Paleozoic chert in the midcontinent, United States: Implications for constraints on diagenetic models*. Bulletin 252, Kansas Geological Survey.

Gassmann, F. (1951). On the elasticity of porous media (M. A. Pelissier, Trans.). In M. A. Pelissier, D. H. Johnston, & J. F. Murphy (Eds.), *Classics of elastic wave theory* (pp. 23–28). SEG Books.

Grammer, G. M., Barnes, D. A., & Harrison, W. B. (2019). Integrated reservoir characterization to provide insight into porosity and permeability distribution in a carbonate mudrock reservoir: Insights from the Michigan Basin, USA. In G. P. Eberli, J. L. Massaferro, & J. F. Sarg (Eds.), *Seismic imaging of carbonate reservoirs and systems* (pp. 189–210). SEPM (Society for Sedimentary Geology)

Gladwin, M. T., & Stacey, F. D. (1974). Anelastic degradation of acoustic pulses in rock. *Physics of the Earth and Planetary Interiors, 8*(4), 332–336.

Gladwin, M. T., & Stagey, F. D. (1974). Ultrasonic pulse velocity as a rock stress sensor. *Tectonophysics, 21*(1-2), 39-45.

Guy, W. J., Byrnes, A. P., Doveton, J. H., & Franseen, E. K. (1999). Prediction of Effective Porosity and Permeability in Mississippian Carbonates, Kansas.

Holubnyak, Y., Watney, W., Rush, J., Fazelalavi, M., & Wreath, D. (2017). Pilot scale CO2 EOR in Mississippian carbonate reservoir at Wellington field in south-central Kansas. *Energy Procedia, 114*, 6989–6996.

Holubnyak, Y. E., Watney, L., Hollenbach, J., Bidgoli, T., Fazelalavi, F. M., Doveton, J., ... & Blazer, B. (2017). *Small scale field test demonstrating CO2 sequestration in Arbuckle Saline Aquifer and by CO2-EOR at Wellington Field, Sumner County, Kansas* (No. DOE-KGS-06821). Univ. of Kansas, Lawrence, KS (United States). Center for Research & Kansas Geological Survey.

Jaeckel, L. (2016). High-resolution sequence stratigraphy and reservoir characterization of Mid-Continent Mississippian carbonates in north-central Oklahoma and south central Kansas [PhD Thesis, Oklahoma State University]. https://search.proquest.com/openview/8078356dc1f6242ae7bbfb5da6975716/1?pq-origsite=gscholar&cbl=18750

Jannsen, D., Voss, J., & Theilen, F. (1985). Comparison of methods to determine Q in shallow marine sediments from vertical reflection seismograms. *Geophysical Prospecting, 33*(4), 479–497. https://doi.org/10.1111/j.1365-2478.1985.tb00762.x

Kansas Geological Survey. *Oil and gas field production query*. Retrieved March 16, 2025, from https://chasm.kgs.ku.edu/ords/oil.ogf4.IDProdQuery?FieldNumber=1000152308

Kelley, V. A., & Saulnier Jr, G. J. (1990). Core analyses for selected samples from the Culebra dolomite at the Waste Isolation Pilot Plant Site. *Sandia National Lab.(SNL-NM), Albuquerque, NM (United States); INTERA, Inc*. https://www.osti.gov/biblio/6127668

King, B. (2013). Fluid flow, thermal history, and diagenesis of the Cambrian-Ordovician Arbuckle group and overlying units in south-central Kansas (Doctoral dissertation, MS thesis, University of Kansas, Lawrence, Kansas).

Krueger, R. C. (1967). Subsurface Study of Mississippian Rocks in the Tulsa Area. https://archives.datapages.com/data/ocgs/data/005/005001/0217.html

Lueck, A., 2017, Characterizing two carbonate formations for CO_2-EOR and carbon geosequestration applicability of existing rock physics models and implications for feasibility of a time lapse monitoring program in the Wellington Oil Field, Sumner County, Kansas [Master's Thesis]: Kansas State University.

Lucia, F. J., Kerans, C., & Jennings, J. W., Jr. (2003). Carbonate Reservoir Characterization. *Journal of Petroleum Technology*, *55*(06), 70–72. https://doi.org/10.2118/82071-JPT

Mavko, G. and Jizba, D., 1991. Estimating grain-scale fluid effects on velocity dispersion in rocks. Geophys., 56, 1940–1949.

Mavko, G., Mukerji, T., & Dvorkin, J. (2020). The rock physics handbook. Cambridge university press. https://books.google.com/books?hl=en&lr=&id=FMS-DwAAQBAJ&oi=fnd&pg=PR11&dq=Mavko,+G.,+Mukerji,+T.,+%26+Dvorking,+J.+(2009).+++The+Rock+Physics+Handbook&ots=u5--hdPCvO&sig=FVHRHd4uN9Ov5gjCYHTQfJK_HLk

Mazzullo, S. J., Wilhite, B. W., Boardman, D. R., Morris, B. T., & Godwin, C. J. (2019). Lithostratigraphy, biostratigraphy, stratigraphic architecture, and depositional systems in Lower to Middle Mississippian strata on the western flank of the Ozark Dome, midcontinent USA. https://archives.datapages.com/data/specpubs/memoir122/data/13996ch02ptg01_025-058.htm

McDonal, F. J., Angona, F. A., Mills, R. L., Sengbush, R. L., Van Nostrand, R. G., & White, J. E. (1958). Attenuation of shear and compressional waves in Pierre Shale. *GEOPHYSICS, 23*(3), 421–439. https://doi.org/10.1190/1.143848

Newell, P., & Ilgen, A. G. (2019). Overview of geological carbon storage (GCS). In *Science of carbon storage in deep saline formations* (pp. 1-13). Elsevier.

Newell, R., Raimi, D., & Aldana, G. (2019). Global energy outlook 2019: the next generation of energy. *Resources for the Future, 1*(8), 1-37.

Ohl, D., & Raef, A. (2014). Rock formation characterization for carbon dioxide geosequestration: 3D seismic amplitude and coherency anomalies, and seismic petrophysical facies classification, Wellington and Anson-Bates Fields, Kansas, USA. *Journal of Applied Geophysics, 103*, 221-231.

Owusu, P. A. (2023), Machine learning in reservoir rocks characterization: Integrating seismic data resolution enhancement for seismic facies classification [Master’s Thesis]: Kansas State University.

Quan, Y., & Harris, J. M. (1997). Seismic attenuation tomography using the frequency shift method. *Geophysics, 62*(3), 895–905. https://doi.org/10.1190/1.1444197

Qi, Q., Fu, L. Y., Deng, J., & Cao, J. (2021). Attenuation methods for quantifying gas saturation in organic-rich shale and tight gas formations. *Geophysics, 86*(2), D65-D75.

Raymer, L. L., Hunt, E. R., & Gardner, J. S. (1980). An improved sonic transit time-to-porosity transform. *SPWLA Trans., 21st Ann. Log. Symp., Paper P*. The Society of Professional Well Log Analyst (SPWLA), Tulsa, OK.

S &P Global. (2016). *An overview of the giant heterogeneous Mississippian carbonate system of the midcontinent: Ancient structure, complex stratigraphy, conventional traps, and unconventional technology in a high fluid volume system.* Retrieved from https://pubs.geoscienceworld.org

Shodunke, G. O. (2021). Reservoir characterization using laboratory ultrasonic rock physics: Understanding pore fluid effects on elastic properties [Masters Thesis]. https://krex.k-state.edu/handle/2097/41000

Simm, R., & Bacon, M. (2014). Seismic amplitude: An interpreter's handbook. *Cambridge university press*. https://books.google.com/books?hl=en&lr=&id=1RYmAwAAQBAJ&oi=fnd&pg=PR9&dq=Simm,+R.,+%26+Bacon,+M.+(2014).+&ots=oBCRmOtKZt&sig=U1iJDkMTBknTZs65HlhLKyruLgU

Smith, T. M., Sondergeld, C. H., & Rai, C. S. (2003). Gassmann fluid substitutions: A tutorial. *Geophysics, 68*(2), 430–440.

Spencer, J. W. (1979). Bulk and shear attenuation in Berea Sandstone: The effects of pore fluids. *Journal of Geophysical Research: Solid Earth, 84*(B13), 7521–7523. https://doi.org/10.1029/JB084iB13p07521

Spikes, K. T., & Dvorkin, J. P. (2005**).** Gassmann-consistency of velocity-porosity transforms. *The Leading Edge, 24*(6), 581–583. https://doi.org/10.1190/1.1926808

Stainsby, S. D., & Worthington, M. H. (1985). Q estimation from vertical seismic profile data and anomalous variations in the central North Sea. *GEOPHYSICS*, *50*(4), 615–626. https://doi.org/10.1190/1.1441937

Teng, T.-L. (1968). Attenuation of body waves and the Q structure of the mantle. *Journal of Geophysical Research*, *73*(6), 2195–2208. https://doi.org/10.1029/JB073i006p02195

U.S. Geological Survey. (n.d.). What is carbon sequestration? *U.S. Department of the Interior*. Retrieved from https://www.usgs.gov/faqs/what-carbon-sequestration

Varela, O. J., Torres-Verdín, C., Sen, M. K., & Roy, I. G. (2006). Using time-lapse seismic amplitude data to detect variations of pore pressure and fluid saturation due to oil displacement by water: a numerical study based on one-dimensional prestack inversion. *Journal of Geophysics and Engineering*, *3*(2), 177.

Vohs, A. B., 2016, 3D Seismic Attributes Analysis in Reservoir Characterization: The Morrison NE Field & Morrison Field, Clark County, Kansas [Master's Thesis]: Kansas State University.

Wang, Z., & Nur, A. (1992). Elastic wave velocities in porous media: A theoretical recipe. *Seismic and Acoustic Velocities in Reservoir Rocks, 2*(10), 1–35.

Wang, Z. Z. (2010). Fundamentals of seismic rock physics. https://pubs.geoscienceworld.org/seg/books/edited-volume/2039/chapter/107760778

Wang, Y., & Lawton, D. C. (2022). Time-lapse attenuation variations during CO2 injection using DAS VSP data from the CaMI Field Research Station, Alberta, Canada. *Second International Meeting for Applied Geoscience & Energy, 538–542*. https://doi.org/10.1190/image2022-3751282.1

Watney, W. L., Guy, W. J., & Byrnes, A. P. (2001). Characterization of the Mississippian chat in south-central Kansas. *AAPG Bulletin*, *85*(1), 85–113.

Wilson, E. N., Watney, W. L., & Grammer, G. M. (2019). An overview of the giant heterogeneous Mississippian carbonate system of the midcontinent: Ancient structure, complex stratigraphy, conventional traps, and unconventional technology in a high fluid volume world.

Winkler, K. W., & Nur, A. (1982). Seismic attenuation: Effects of pore fluids and frictional-sliding. *GEOPHYSICS, 47*(1), 1–15. https://doi.org/10.1190/1.1441276

Wittman, B. R. (2013). Subsurface stratigraphy and characterization of Mississippian (Osagean to Meramecian) carbonate reservoirs of the northern Anadarko Shelf, north-central Oklahoma. University of Arkansas. https://search.proquest.com/openview/82a409a4b238e743adbe1482087c2e99/1?pq-origsite=gscholar&cbl=18750

Wojcik, K. M. (1992). Diagenesis of Pennsylvanian sandstones and limestones, Cherokee basin, southeastern Kansas: Importance of regional fluid flow (Doctoral dissertation, University of Kansas).

Wyllie, M. R. J., Gregory, A. R., & Gardner, L. W. (1956). Elastic wave velocities in heterogeneous and porous media. *Geophysics, 21*(1), 41-70. https://doi.org/10.1190/1.1438217

Xu, S., & Payne, M. A. (2009). Modeling elastic properties in carbonate rocks. *The Leading Edge, 28*(1), 66–74.

Yale, D. P., & Jamieson, W. H. (1994). Static and dynamic rock mechanical properties in the Hugoton and Panoma fields, Kansas. *SPE Oklahoma City Oil and Gas Symposium/Production and Operations Symposium, SPE-27939*. https://onepetro.org/SPE

Young, E. M. (2010). Controls on reservoir character in carbonate-chert strata, Mississippian (Osagean-Meramecian), southeast Kansas (Doctoral dissertation, University of Kansas).

Zhang, C., & Ulrych, T. J. (2002). Estimation of quality factors from CMP records. *Geophysics, 67*(5), 1542-1547.

Appendix A -

	Sample	Density of dry sample	Vs^2	Vp^2	Shear modulus	Bulk modulus	
	3718.7	**2.728142857**	**4797765**	**23025348**	**13088988**	**3486828**	
	3734.2	**2.6505**	**5955553**	**34277285**	**15785194**	**9237056**	
	4076.5	**2.747857143**	**5536692**	**36112481**	**15214039**	**12791927**	
	4096.2	**2.482142857**	**5684979**	**36721182**	**14110931**	**11567832**	
	3936.6	**2.610375**	**6069383**	**32765220**	**15843366**	**7385349**	
Sample	**Density of brine saturated**						
3734.2	**2.6505**						
4096.2	**2.482143**						
4076.5	**2.747857**						
3718.7	**2.728143**						
3936.6	**2.610375**						

Appendix Table 1 Bulk moduli of each sample needed to compare with Mavko-Jizba model

Appendix B -

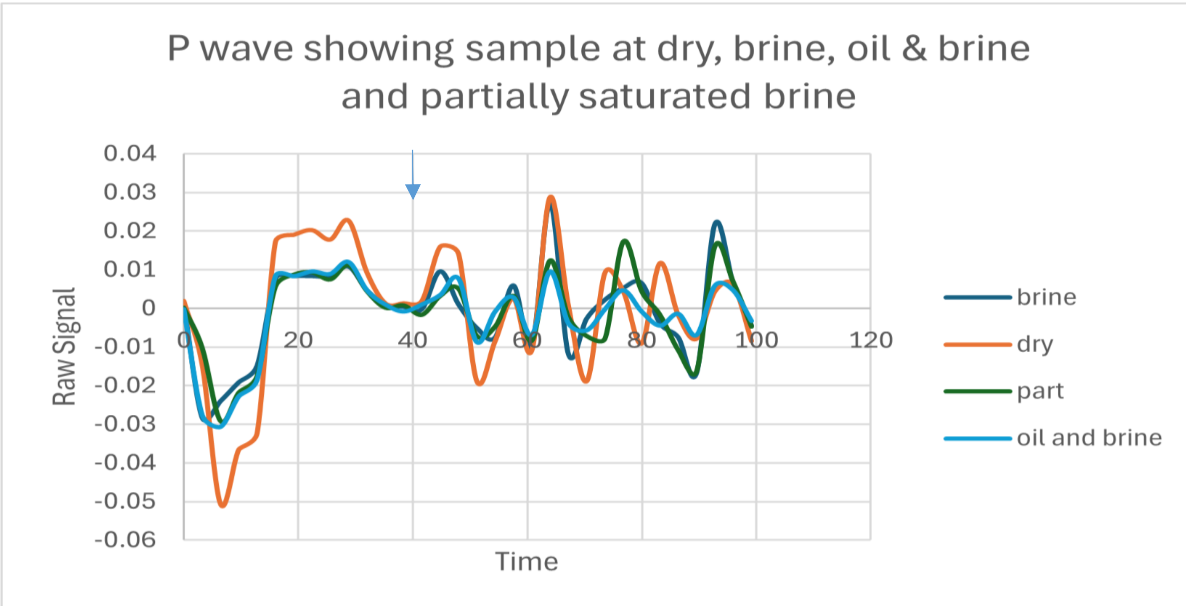

Appendix Figure 6.1Sample 3717.8 Graph showing P waves superimposed for dry, oil, brine and partially saturated brine sample at same frequency and first arrival time(arrow).

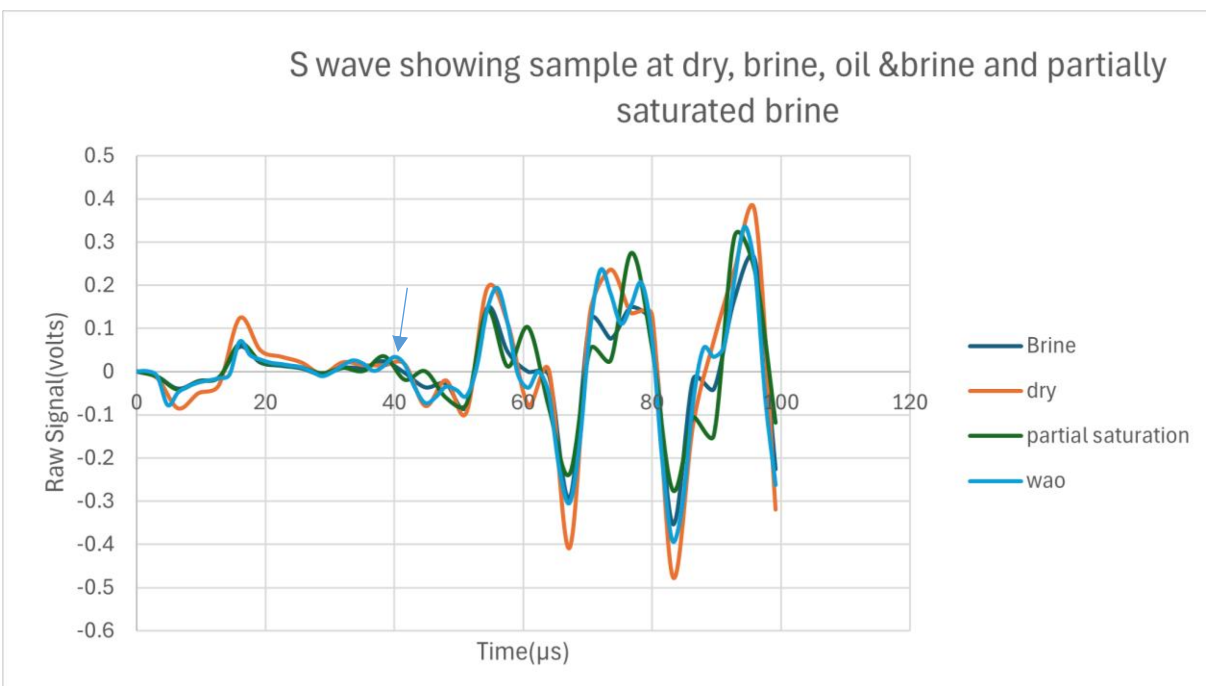

Appendix Figure 6.2 Sample 3717.8 Graph showing S waves superimposed for dry, oil, brine and partially saturated brine sample at same frequency and first arrival time(arrow).

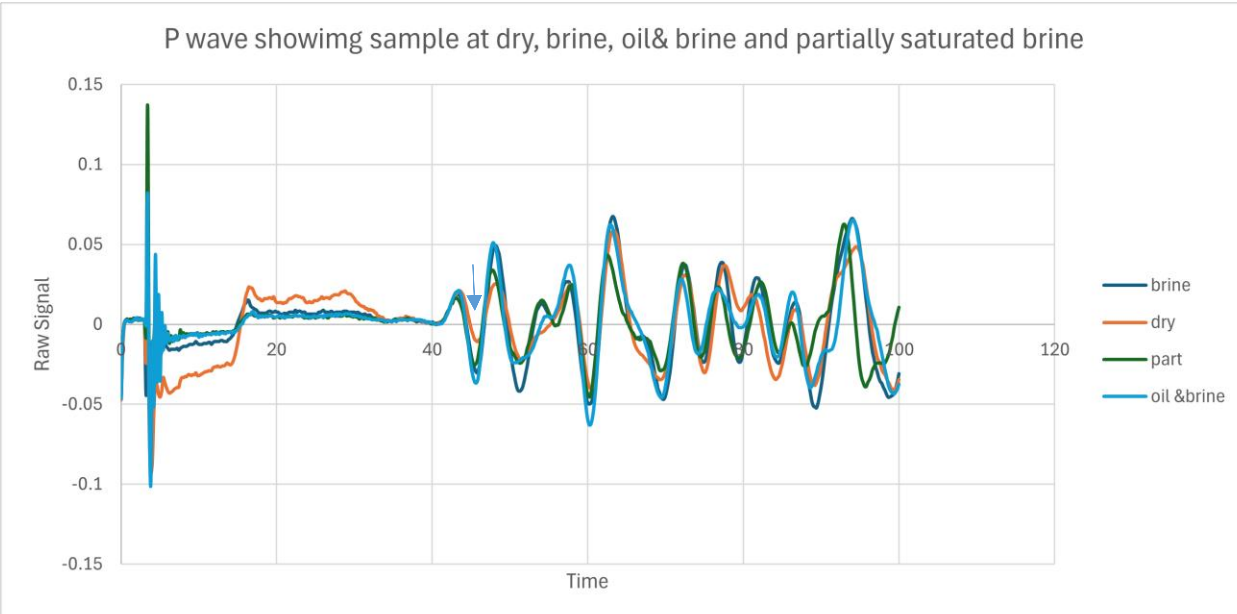

Appendix Figure 6.3 Sample 3936.6 Graph showing P waves superimposed for dry, oil, brine and partially saturated brine sample at same frequency and first arrival time(arrow).

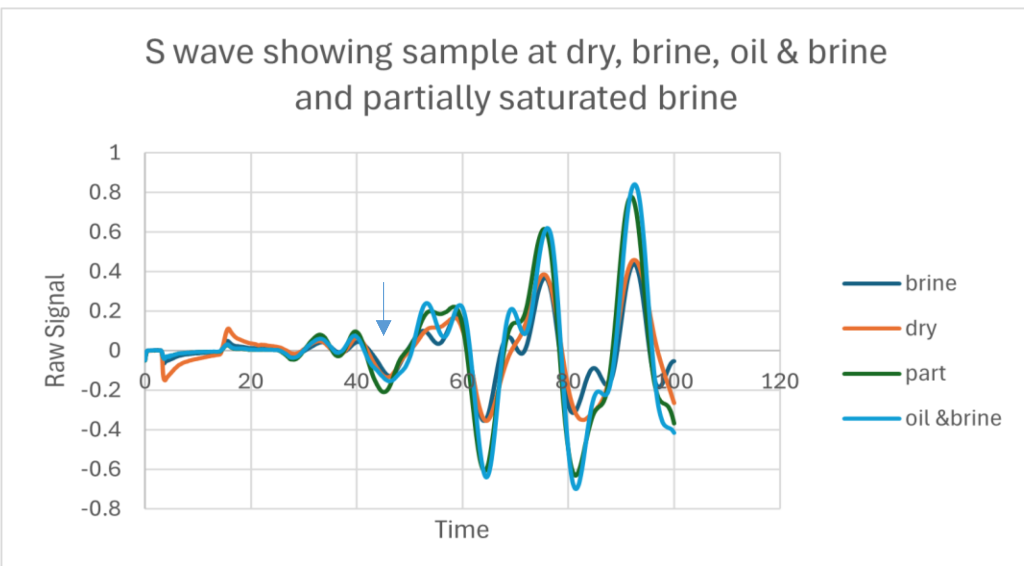

Appendix Figure 6.4 Sample 3936.6 Graph showing S waves superimposed for dry, oil, brine and partially saturated brine sample at same frequency and first arrival time(arrow).

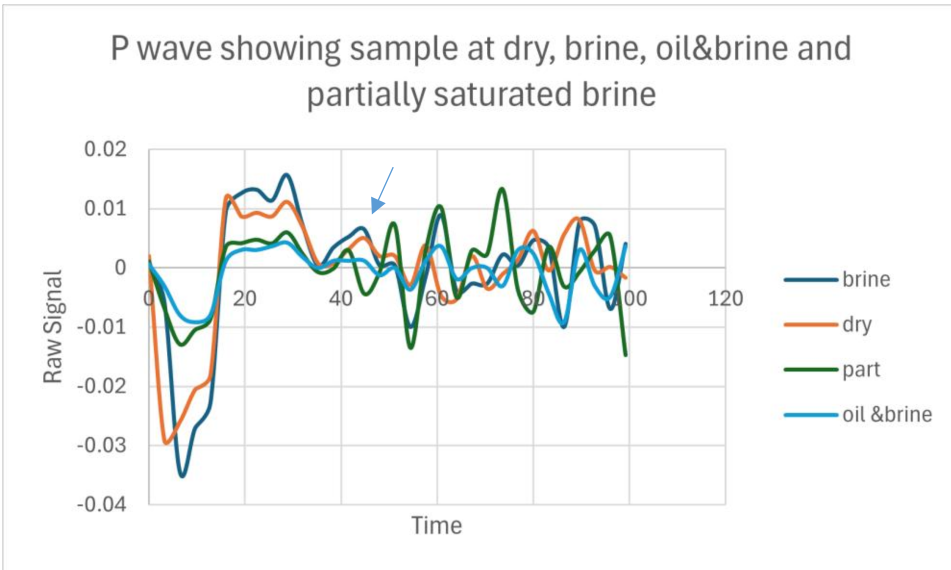

Appendix Figure 6.5 Sample 4076.5 Graph showing P waves superimposed for dry, oil, brine and partially saturated brine sample at same frequency and first arrival time(arrow).

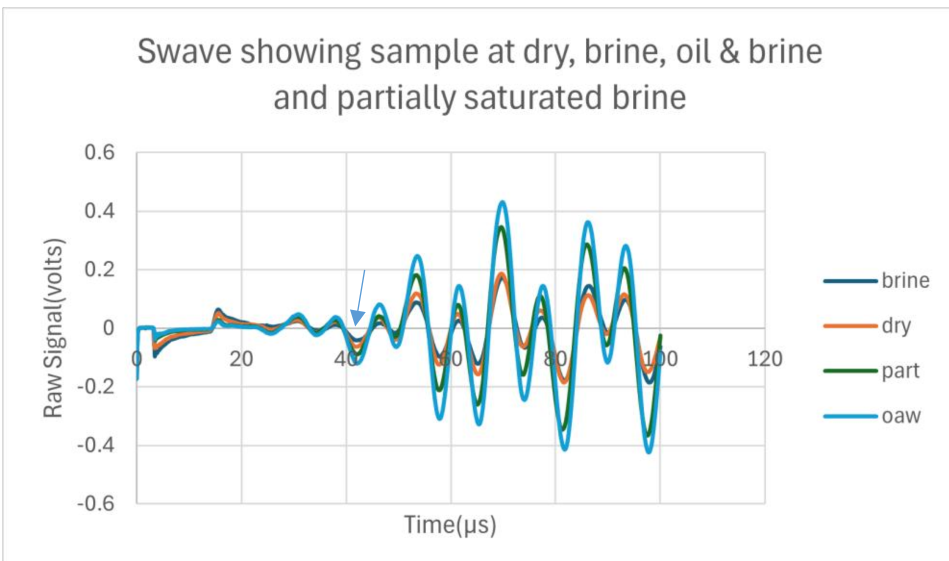

Appendix Figure 6.6 Sample 4076.5 Graph showing S waves superimposed for dry, oil, brine and partially saturated brine sample at same frequency and first arrival time(arrow).

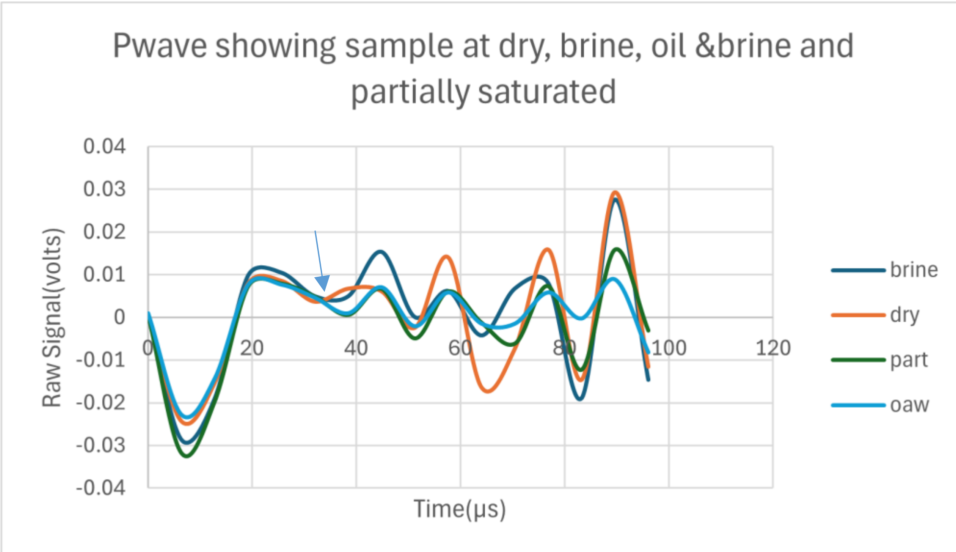

Appendix Figure 6.7 Sample 4096.2 Graph showing P waves superimposed for dry, oil, brine and partially saturated brine sample at same frequency and first arrival time(arrow).

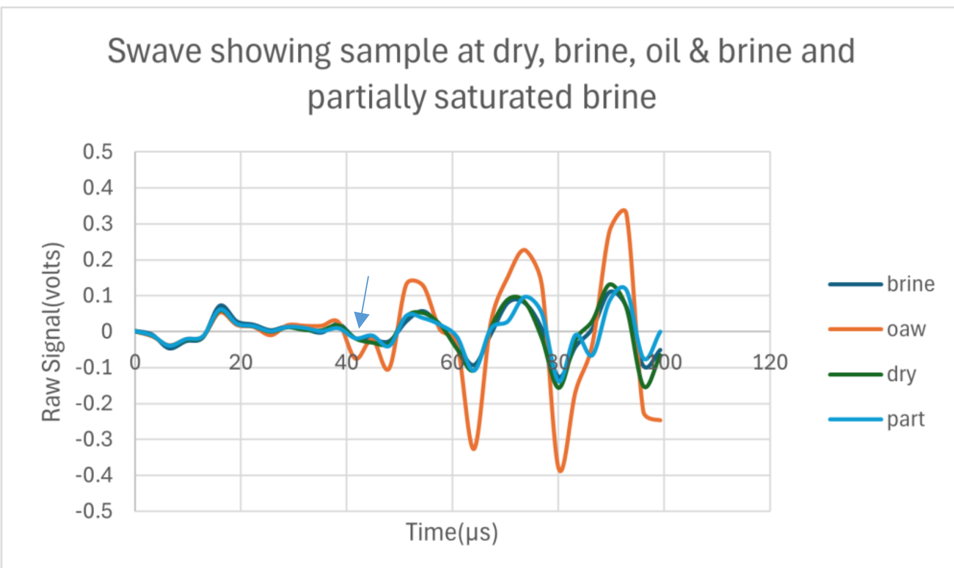

Sample 4096.2 Graph showing S waves superimposed for dry, oil, brine and partially saturated brine sample at same frequency and first arrival time(arrow).